Massive MIMO Channel Modeling

Xin You
carolineyou@sina.com
Yongchun Wang
w_yongchun@sina.com

Department of Electrical and Information Technology
Lund University

Advisor: Xiang Gao, Ove Edfors

December, 2015

Printed in Sweden
E-huset, Lund, 2015

Abstract

Massive MIMO has attracted many researchers' attention as it is a promising technology for future 5G communication systems. To characterize the propagation channels of the massive MIMO and to evaluate system performance, it is important to develop an accurate channel model for it.

In this thesis, two correlative models, i.e., the Kronecker model and the Weichselberger model, and a cluster-based model, i.e., the Random Cluster Model (RCM), have been validated based on real-life data from four measurement campaigns. These measurements were performed at Lund University using two types of base station (BS) antenna arrays, a practical and compact uniform cylindrical array (UCA) and a physically-large virtual uniform linear array (ULA), both at 2.6 GHz.

For correlative models, performance metrics such as channel capacity, sum-rate and singular value spread are examined to validate the model. The random cluster model, which is constructed and evaluated on a cluster level, has been parameterized and validated using the measured channel data.

The correlative models are relatively simple and are suitable for analytical study. Validation results show that correlative models can reflect massive MIMO channel capacity and singular value spread, when the compact UCA is used at the base station and when users are closely located. However, for the physically-large ULA, correlative models tend to underestimate channel capacity. The RCM is relatively complex and is usually used for simulation purpose. Validation results show that the RCM is a promising model for massive MIMO channels, however, improvements are needed.

Key words: massive MIMO, 5G, channel modeling, the Kronecker model, the Weichselberger model, capacity, sum-rate, singular value spread, the Random Cluster Model, cluster, spatial correlation, large-scale fading

Acknowledgement

We would like to show our sincere gratitude to our advisor Xiang Gao for her patient guidance and insightful comments during the thesis project, which helped us a lot to finish our report.

Our genuine appreciation also goes to our supervisor Prof. Ove Edfors, who give us the opportunity to join this excellent project, and helped us get through the difficulties.

Then we sincerely thank our examiner Fredrik Rusek for the feedback and suggestion of our thesis report.

Special thanks should go to our friend Jing who has put considerable time and effort into her comments on the draft.

We would also like to thank our family and friends who give us support, and encouragement all the time.

Lund, December 2015
Xin You and Yongchun Wang

Table of Contents

1 Introduction **1**
- 1.1 Massive MIMO Background . . . 1
- 1.2 MIMO Channel Models . . . 3
- 1.3 Tesis Structure . . . 6

2 Massive MIMO Measurements **7**
- 2.1 Measurement Setups . . . 7
- 2.2 Measurement Campaigns . . . 8

3 Correlative Channel Models **13**
- 3.1 Formula Derivation . . . 13
- 3.2 Validation Metrics . . . 18

4 Validation of Correlative Models **21**
- 4.1 Linear Array . . . 21
- 4.2 Cylindrical Array . . . 29

5 Summary Results of the Correlative Models **59**
- 5.1 Linear Array . . . 59
- 5.2 Cylindrical Array . . . 61

6 Random Cluster Model **67**
- 6.1 Measurement Data Processing . . . 67
- 6.2 Parametric Model . . . 67
- 6.3 Birth-Death Process . . . 69
- 6.4 System Model . . . 72
- 6.5 Model Validation . . . 72

7 Conclusions and Discussion **79**

References 81

List of Figures 83

List of Tables 91

List of Abbreviations 95

Chapter 1

Introduction

1.1 Massive MIMO Background

With the development of wireless communication systems, the demands for high data rate and link reliability of the communication systems also increase. One of the trends is going from single antenna to multiple antennas, so called multiple-input multiple-output (MIMO) [1]. Because of its advantages in terms of improved capacity and link reliability, MIMO technology has been widely studied in the past and used in various standards such as Universal Mobile Telecommunication System (UMTS) and Long Term Evolution (LTE) [2].

The first studies were focused on point-to-point MIMO links, which is called conventional MIMO. In conventional MIMO where two devices transmit and receive with a relatively small number of antennas, each transmit antenna will be deployed with one transmit RF chain [3]. In recent years, the focus has shifted to conventional multi-user MIMO (MU-MIMO) where a base station (BS) equipped with multiple antennas simultaneously serves multiple single-antenna users and thereby achieves multiplexing gain. This way offers some big advantages over conventional point-to-point MIMO: user terminals can work with cheap single-antenna transceivers and most of the expensive equipment can be placed at the BS. Another important advantage of MU-MIMO is their ability to achieve diversity, which makes the performance of the system become more robust to the propagation environment. Because of these advantages, MU-MIMO is progressively being employed throughout the world and has developed as a part of communications standards, such as LTE, 802.11 (WiFi) and 802.16 (WiMAX).

In the next generation cellular networks, higher user densities and increased data rates are required. Due to the BS typically employs a few antennas for most regular MU-MIMO systems, it limits the experienced increase of data rates and thereby the achieved spectral efficiencies. Re-

searchers are thinking of increasing the number of antennas at the BS to boost the system performance.

The deployment of conventional MU-MIMO systems with a large number of (tens to hundreds) antennas at the BS is known as massive MIMO in the literature [4]. It is an emerging technology and has attracted significant attention in the research community due to the following main advantages:

- **Spectral efficiency:** It has been shown that massive MIMO is a good technology for enhancing spectral efficiency (bit/s/Hz/cell). This is achieved by massive arrays and simultaneous beamforming to users so that the received multipath components of the wanted signal adds up coherently while the remaining part of the signal does not. Together the antenna elements can achieve unprecedented array gains and spatial resolution, which will result in robustness to inter-user interference and increase the number of simultaneously served users per cell. Compared to a single-antenna system, massive MIMO is assumed to improve spectral efficiency by at least an order of magnitude [5–7].

- **Interference reduction:** The interference from other co-channel users may significantly degrade the performance of a targeted user. Massive MIMO tackles this question by using interference reduction or cancellation techniques, such as dirty paper coding (DPC) for the downlink and maximum likelihood (ML) multiuser detection for the uplink. However, these technques are complex and suffer high computational complexity. [8]

- **Transmit-Power efficiency:** The massive MIMO technology described in [9] improves transmit-power efficiency due to diversity effects and array gains. The power scaling law for massive MIMO systems has been derived in [10]. It shows that, to achieve the performance equal to a single-input single-output (SISO) system, the transmit power of each single-antenna user in a massive MIMO system can be scaled down proportionally to the number of BS antennas if the BS acquires perfect channel state information (CSI) or to the square root of the number of BS antennas if the BS has imperfect CSI [10]. This is the one of the important advantage of massive MIMO and the potential for improving transmit-power efficiency is huge.

- **Link reliability:** It is conceivable that a large number of degrees of freedom can be provided by the propagation channel due to the number of antennas at the transmitter and receiver is typically assumed

to be larger. The more degrees of freedom the better link reliability and the higher data rate [11].

With the above advantages, massive MIMO systems is widely considered as a promising enabler for the 5G mobile communications.

1.2 MIMO Channel Models

In most cases, MIMO channels leads to the increased capacity compared to SISO channels due to the assumption that the MIMO paths are uncorrelated. The assumption has been flattened in [12]. It also has shown that the capacity of a measured channel is commonly less than the limit according to the environment. Since channel model is the deterministic portion of the whole system and their performance depends on the environment, accurate models are highly needed.

In general, there are two purposes served by MIMO channel models. In the first place, the models play as a channel simulator. A MIMO system can be designed by employing a MIMO channel model in terms of the design for signalling schemes, detection schemes and space-time codes. As a result, the same model can be applied to evaluate properly the performance of a given system and build exemplar channels. In the second place, an accurate channel model results in a relatively deep insight into the underlying physics of the channel. It not only is good for the behaviour of a given channel analysis, but also makes safe assumptions in system design.

To characterize massive MIMO channels and to evaluate system performance, it is important to develop an accurate model for it. Here, we study two classes of MIMO channel models, correlative models and cluster model, by using the measured channel data. The measurements for massive MIMO will be briefly introduced in the Chapter 2.

1.2.1 Correlative Models

Various correlative models have been proposed for MIMO such as the Kronecker, Weichselberger and Structured models. We focus on the first two models in this thesis.

The Kronecker Model The Kronecker model is studied at first due to its simplicity as shown Figure 1.1. It greatly reduces the complexity of the channel analysis, as it holds the assumption that the correlation between the receive antennas is independent of the correlation among the transmit antennas.

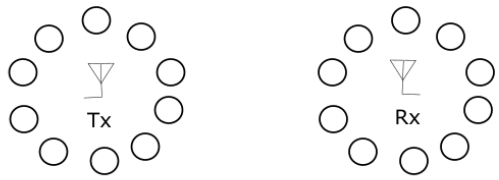

Figure 1.1: Transmit correlation only depends on the scattering at the transmit side, and correspondingly, receive correlation only relies on the scattering at the receive side.

In our work, the main task is to model the spatial correlation between massive MIMO sub-channels within the framework of the Kronecker model without the impact of antenna coupling. The massive MIMO channel model takes into account the correlation by treating the fixed correlation at the receiver and transmitter following the well-known Kronecker model given by [13]

$$\mathbf{H}_{\text{kron}} = \mathbf{R}_{\text{Rx}}^{1/2}\mathbf{G}\mathbf{R}_{\text{Tx}}^{1/2} \tag{1.1}$$

where the channel matrix $\mathbf{G}$ is populated with independent and identically distributed (i.i.d.) zero-mean complex-Gaussian entries. The $\mathbf{R}_{\text{Rx}}^{1/2}$ and $\mathbf{R}_{\text{Tx}}^{1/2}$ are the matrix square-roots of the receive-correlation matrix $\mathbf{R}_{\text{Rx}}$ and the transmit-correlation matrix $\mathbf{R}_{\text{Tx}}$, respectively.

The advantage of the Kronecker model is its simplicity, and it is often used for analytical study of MIMO systems. However, due to the assumption of no coupling between the transmit and receive sides, the model may not be accurate enough for some propagation environments.

The Weichselberger Model A relatively more complex correlative model, i.e., the Weichselberger model, can be more accurate than the Kronecker model as it introduces coupling effect between the propagation at the transmit and receive sides [14, 15]. The model can be represented in [15] as follows:

$$\mathbf{H}_{\text{weich}} = \mathbf{U}_{\text{Rx}}(\widetilde{\mathbf{\Omega}} \odot \mathbf{G})\mathbf{U}_{\text{Tx}}^{T} \tag{1.2}$$

where $\mathbf{G}$ denotes a random matrix with i.i.d complex-Gaussian entries. $\mathbf{U}_{\text{Rx}}$ and $\mathbf{U}_{\text{Tx}}$ are the one-sided eigenvectors. $\odot$ is the element-wise product of two matrices (or the Hadamard product), and $\widetilde{\mathbf{\Omega}}$ is the element-wise square root of the power coupling matrix $\mathbf{\Omega}$.

The Weichselberger model suggests the opposite assumption relative to the Kronecher model [14]; scatters at the two link ends cannot be considered independent and are coupled in some way. Because of this reason, the Weichselberger model is more accurate, when compared with the Kronecker model. However, additional complexity is required to define the power coupling matrix.

1.2.2 Cluster Models

Cluster models, usually geometry-based, are based on the concept of clusters. A cluster is defined as a group of multipath components (MPCs) with similar parameters, such as angles of arrival (AOA), angles of departure (AOD) and delays. Cluster models simulate channels based on clusters through a set of stochastic parameter. One significant difference between the cluster-based models and the correlatives models is that cluster models capture the time-variant nature of the radio channel. The most well-known cluster models are the Saleh-Valenzuela model, the 3GPP Spatial Channel Model (SCM), the Wireless World Initiative New Radio II (WINNER II) channel model, the COST 273 Model and the Random Cluster Model (RCM). In this thesis, we focus on the RCM. [13]

The Random Cluster Model The random cluster model defined in [16] is a geometry-based stochastic MIMO channel model (GSCM). It emerged from the COST 273 MIMO Channel Model [13] with two considerable improvements: (i) the cluster parameters are obtained by statistical data, (ii) the environment PDF is applied to characterize the cluster parameters.

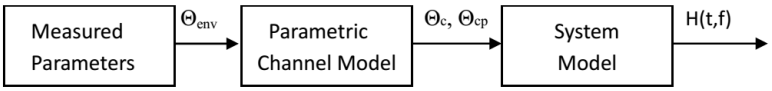

Figure 1.2: The RCM framework

As shown in Figure 1.2, there are three main parts in the RCM basic framework. Firstly for the measured parameters, a multivariate probability density function (PDF) called the environment PDF $\boldsymbol{\Theta}_{\text{env}}$ is applied to describe the clusters parameters extracted from measured data statistically.

Next, in the parametric channel model, we use the obtained $\mathbf{\Theta}_{\text{env}}$ to generate the cluster parameter sets $\mathbf{\Theta}_c$ and multipath component parameter sets $\mathbf{\Theta}_{c,p}$. With the parameters obtained from the environment PDF $\mathbf{\Theta}_{\text{env}}$, channel matrices can be generated through the system model.

For the RCM, one of the greatest strengths is that a time-variant channel is simulated by tracking the clusters over time domain. Secondly, the model is simplified by using the environment PDF to characterize the channels. However, the process of computing the environment PDF is intricate. How to define and clustering the clusters from the measurement data still need to be optimized.

1.3 Tesis Structure

In this thesis, based on real-life channel data, we investigate the suitability of three channel models for massive MIMO, e.g., the Kronecker model, the Weichselberger model, and the RCM. In order to validate the studied channel models and compare with the measured massive MIMO channels, on one hand, we evaluate the Kronecker model and the Weichselberger model by comparing the uplink capacity, zero-forcing (ZF) sum-rate and the singular value to the measured channel; on the other hand, we validate the correlation properties and channel fading process for both the RCM and measured channel.

This thesis report is organised as follows: Chapter 2 will give the description of four measurement campaigns for massive MIMO channels, based which we construct and validate the above-mentioned models. In Chapter 3, the formula deviation for the correlative models and several performance metrics will be presented. The validation results and analysis for the correlative models will be shown in Chapter 4 and Chapter 5. In Chapter 6, the process of establishing the RCM will be described in detail, and the validation results in terms of spatial correlation and large-scale fading properties will be reported. Chapter 7 will give conclusions and discussion for this thesis work.

Chapter 2

Massive MIMO Measurements

As mentioned previously, the channel models constructed in this thesis are based on real environment channel measurements. For the massive MIMO measurement campaigns, the measurement setups, the measurement environments as well as the measurement scenarios will be presented in this chapter. The selected measurement campaigns have been first reported in [17–19], here gives a brief description, which is focused on their major parameters.

2.1 Measurement Setups

Two different kinds of large arrays, practical uniform cylindrical array (UCA) and virtual uniform linear array (ULA), have been employed as the BS in the measurement campaigns, shown in Figure 2.1. Both large antenna arrays comprise 128 antenna elements with a adjacent space of half a wavelength at 2.6 GHz.

As shown in Figure 2.1a, the cylindrical antenna array consists of 64 dual-polarized directional patch antennas arranged in four circles, which is total 128 antenna ports. Each circles of the antenna array are stacked on top of each other and the array gives a physical size of 29.4 cm for the diameter and 28.3 cm for the height. By using the RUSK LUND MIMO channel sounder, the measurement can be recorded at center frequency 2.6 GHz.

In the right hand side of Figure 2.1, a virtual uniform linear array with a moving vertically-polarized omni-directional antenna is shown. The antenna shifts with 128 isometric points along the rail. A HP 8720C vector network analyzer (VNA) was applied to record the measurement data using a center frequency of 2.6 GHz. By comparing the dimension of UCA and ULA, ULA is almost 25 times of UCA, which suffers 7.4 m long.

a) Cylindrical array b) Linear array

Figure 2.1: Two large antenna arrays: a) practical uniform cylindrical array (UCA), and b) virtual uniform linear array (ULA).

2.2 Measurement Campaigns

The channel measurement campaigns were took place at the campus of the Faculty of Engineering (LTH), Lund University, Sweden (55.711510 N, 13.210405 E). Four massive MIMO measurement campaigns are selected to represent both the virtual user and the fully-synchronous user, and also the measurement environment of indoor and outdoor, namely the "ULA with 5 virtual users", the "UCA with 5 virtual users", the "UCA with 9 synchronized users - outdoor", and the "UCA with 9 synchronized users - indoor".

2.2.1 ULA with 5 Virtual Users

In this scenario, the user side equipped an omni-directional antenna with vertical polarization as the receiver. And the ULA at the BS was placed at the roof of E-building of LTH, which plays the role of transmitter. The measurement campaign was processed during the night aiming to get a static channel.

Figure 2.2 gives an overview of the semi-urban measurement area, which contains the position of BS and 8 measurement sites (MS) of user side. Within these sites, 3 (MS 1-3) have line-of-sight (LOS) condition and 4 (MS 5-8) have non-line-of-sight (NLOS) condition. The LOS component of site MS 4 was blocked by the edge of the roof. For each site, 5 positions with a inter-spacing of 0.5-2 m have been measured. The channel data were recorded with the VNA at center frequency 2.6 GHz and 50 MHz bandwidth, each measurement suffered about half an hour to record.

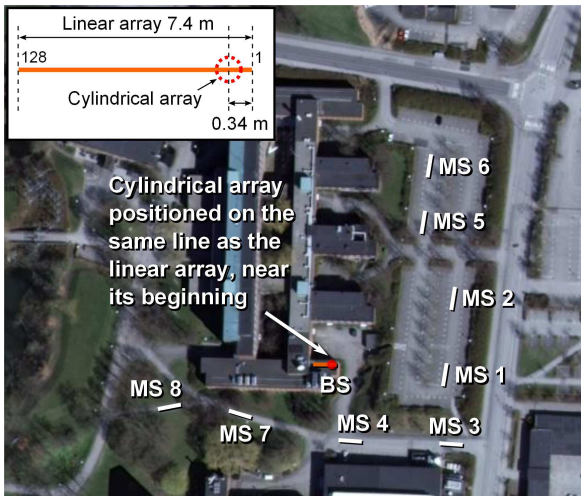

Figure 2.2: Overview of the measurement area at the campus of the Faculty of Engineering (LTH), Lund University, Sweden. Two BS large antenna arrays were placed at the same roof of E-building of LTH during the two respective measurement campaigns, 8 MS sites were measured.

2.2.2 UCA with 5 Virtual Users

This scenario gives similar setup with the former scenario, an omni-directional antenna with vertical polarization was deployed at the user side as the receiver. The UCA, which is the BS, placed at the same roof of E-building of LTH as ULA. Due to its compactness, the UCA was placed at the beginning of the ULA, shown in the top left corner of Figure 2.2.

The user (an omni-directional antenna) moved around the 8 user sites (MS 1-8) , four of the sites (MS 1-4) have LOS condition, while the other four (MS 5-8) have NLOS condition. 40 positions were measured with a inter-spacing of 0.5 m, and the data were recorded by the RUSK LUND MIMO channel sounder at center frequency 2.6 GHz and 50 MHz bandwidth.

2.2.3 UCA with 9 Synchronized Users - Outdoor

In this measurement campaign, nine vertically-polarized omni-directional antennas performed as nine simultaneous users. At the BS side, a UCA was installed at the low roof (two floors) of E-building of LTH. During the measurement, the 9 users were moving randomly inside a circle with a 5 m diameter, at a speed of about 0.5 m/s (see Figure 2.3b). To get both vertical and horizontal polarizations, the users were asked to hold the

Figure 2.3: UCA with 9 synchronized users - outdoor measurement (a) The measurement area, (b) The users moving randomly in a 5 m diameter circle.

antennas with a angle of inclination (45 degrees). Except the non-crowd condition, the heavy crowd condition with 10 - 12 persons walking around the 9 users in the circle has also been considered. [20]

As shown in Figure 2.3a, the BS location and 4 sites with different propagation conditions of user side (MS 1-4) were labeled. MS 1 and MS 2 have LOS condition, MS 3 and MS 4 have NLOS condition. The RUSK LUND MIMO channel sounder was connected to record the measurement data at 2.6 GHz center frequency and 40 MHz bandwidth. At each measurement, 300 snapshots were recorded during a measurement period of 17 seconds. [19]

2.2.4 UCA with 9 Synchronized Users - Indoor

This measurement were performed in an auditorium of E-building of LTH, which represents a indoor duplicate scenario of the "UCA with 9 synchronized users - outdoor" scenario. The cylindrical array at the BS side was fixed at a height of 3.2 m. For the user side, 9 users were sited randomly in 20 seats. Each of them held a vertically-polarized omni-directional antenna either vertically or tilted 45 degrees during different measurements, and the users were asked to move the antenna arbitrary with a speed less than 0.5 m/s. Besides including the non-crowd case with only 9 active users sitting among the 20 seats, the heavy crowded condition were performed with additional 11 non-active users to fill the 20 seats (see Figure 2.4b).

Figure 2.4a shows an overview of the measurement area. 4 BS positions and 2 groups of users in both middle and back of the auditorium have been

measured respectively. The channel sounder named RUSK LUND MIMO was appointed to record the measurement data followed the conditions, which are 2.6 GHz center frequency and 40 MHz bandwidth. In order to record each measurement, 300 snapshots were recorded within the period of 17 seconds.

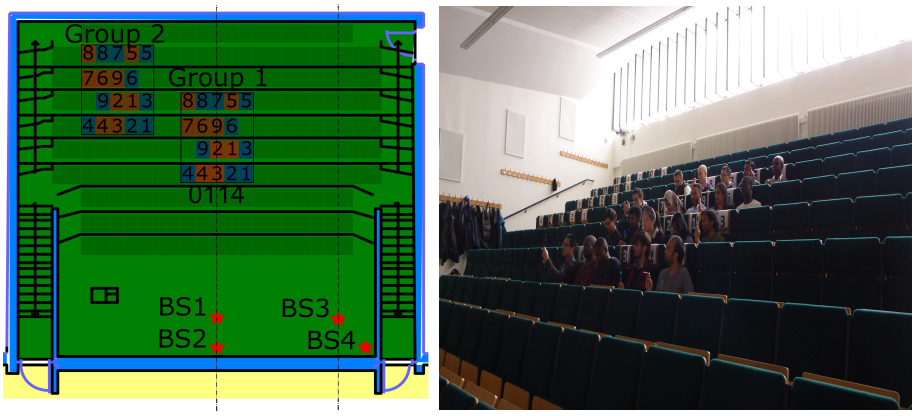

(a) **(b)**

Figure 2.4: UCA with 9 synchronized users - indoor measurement (a) The measurement area, (b) The users.

Chapter 3

Correlative Channel Models

3.1 Formula Derivation

It is important to highlight the significant drawback of the full correlation matrix, which is the huge size of parameters. The correlative channel models, the Kronecker and Weichselberger, overcome the drawback by decomposing the full correlation using the parameterized one-sided correlation matrices.

The Kronecker model
For the massive MIMO measurement, the narrowband channel gain matrix $\mathbf{H}_{\ell,n}$ is given by the Equation 3.1 for convenience of presentation. The $\mathbf{H}_{\ell,n}$ is the channel matrix at subcarrier ℓ and snapshot n, that is

$$\mathbf{H}_{\ell,n} = \begin{pmatrix} h_{11} & \cdots & h_{1M} \\ \vdots & \ddots & \vdots \\ h_{K1} & \cdots & h_{KM} \end{pmatrix} \tag{3.1}$$

According to the definition in [21], the covariance of the channel can be formulated using the measured channel matrix as

$$\mathbf{R}_{H,\ell} = E\{\mathrm{vec}(\mathbf{H}_\ell)\mathrm{vec}(\mathbf{H}_\ell)^H\} \tag{3.2}$$

where $\mathbf{R}_{H,\ell} \in \mathcal{C}^{\mathcal{K}\times\mathcal{M}}$ is a positive semi-definite (PSD) Hermitian matrix, $\mathrm{vec}(\mathbf{H}_\ell)$ is to stack $\mathbf{H}_\ell$ into a vector columnwise, and $(.)^H$ stands for conjugate transpose operation.

The Kronecker model assumes that the separate spatial correlation structure at the transmitter and receiver sides can be described by the transmit-correlation and receive-correlation matrices. It means that the two correlation matrices are not coupled in any cases. As mentioned in [13],

the narrowband receive-correlation matrix $\mathbf{R}_{\mathrm{Rx}} \in \mathcal{C}^{\mathcal{K}\times\mathcal{K}}$ can be achieved as follows

$$\begin{aligned}\mathbf{R}_{\mathrm{Rx},\ell} &= \frac{1}{N}\sum_{n=1}^{N}\{\mathbf{H}_{n,\ell}\mathbf{H}_{n,\ell}^{H}\} \\ &= E\{\mathbf{H}_{\ell}\mathbf{H}_{\ell}^{H}\}\end{aligned} \tag{3.3}$$

The narrowband transmit-correlation matrix $\mathbf{R}_{\mathrm{Tx}} \in \mathcal{C}^{\mathcal{M}\times\mathcal{M}}$ is achieved as Equation 3.4

$$\begin{aligned}\mathbf{R}_{\mathrm{Tx},\ell} &= \frac{1}{N}\sum_{n=1}^{N}\{\mathbf{H}_{n,\ell}^{T}\mathbf{H}_{n,\ell}^{*}\} \\ &= E\{\mathbf{H}_{\ell}^{H}\mathbf{H}_{\ell}\}^{T}\end{aligned} \tag{3.4}$$

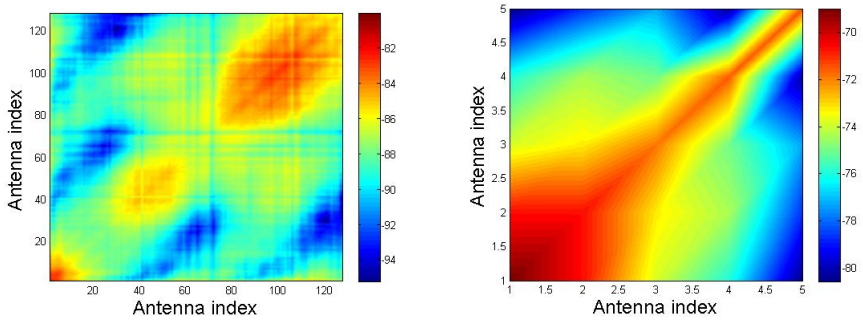

Figure 3.1: The transmit-correlation matrix (left) and the receive-correlation matrix (right). Measurement campaign: ULA with 5 virtual users; User location: MS 2; Propagation condition: LOS.

Figure 3.1 and Figure 3.2 show one-sided correlation matrices of two selected scenarios from the measurement campaign performed with linear array. Since the assumption for Kronecker model is that the correlation matrix $\mathbf{R}_H$ can be expressed as the Kronecker product of the one-sided correlation matrices, the kronecker structure for modeling the channel can be written as below

$$\mathbf{R}_{H,\ell} = \mathbf{R}_{\mathrm{Rx},\ell} \otimes \mathbf{R}_{\mathrm{Tx},\ell} \tag{3.5}$$

where $\otimes$ stands for the Kronecker product.

With respect to model the channel covariance, we prefer to use this model. As stated in the above, the one-sided correlation matrices are separable. This assumption not only reduces the number of parameters, which is

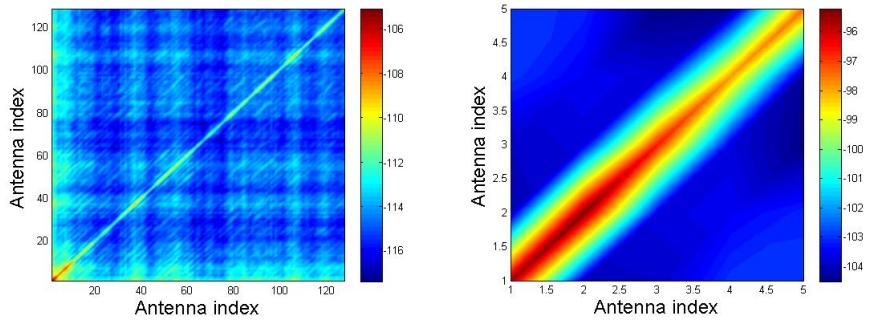

Figure 3.2: The transmit-correlation matrix (left) and the receive-correlation matrix (right). Measurement campaign: ULA with 5 virtual users; User location: MS 5; Propagation condition: NLOS.

used to describe the correlation, but also justifies the truth that the antenna arrays are separated by a large distance and there are enough random scattering between them. Therefore, the Kronecker model considers the same spatial structure as the measured channel $\mathbf{H}_{\ell,n}$ and can be expressed as

$$\mathbf{H}_{\mathrm{Kron},\ell} = \mathbf{R}_{\mathrm{Rx},\ell}^{1/2} \mathbf{G}_\ell \mathbf{R}_{\mathrm{Tx},\ell}^{1/2} \tag{3.6}$$

where $\mathbf{R}_{\mathrm{Rx},\ell}^{1/2}$ and $\mathbf{R}_{\mathrm{Tx},\ell}^{1/2}$ are the matrix square-roots of the transmit covariance matrix $\mathbf{R}_{\mathrm{Rx},\ell}$ and the receive covariance matrix $\mathbf{R}_{\mathrm{Tx},\ell}$, respectively, both $\mathbf{R}_{\mathrm{Rx},\ell}$ and $\mathbf{R}_{\mathrm{Tx},\ell}$ are PSD Hermitian matrices, and $\mathbf{G}_\ell \in \mathcal{C}^{\mathcal{K}\times\mathcal{M}}$ is the i.i.d matrix with zero-mean, unit variance circularly-symmetric complex Gaussian distributed entries [13].

From the previous steps, the Kronecker channel model can be built based on the data of the massive MIMO measurement. In fact, it was proposed that the Kronecker model will result in an underestimation of the MIMO mutual information due to it cannot generate an actual channel [14]. In this thesis, this fact has been explained and the results will be displayed in the next chapter.

The Weichselberger model

In contrast to the Kronecker model, the Weichselberger model generates a correlative model from measurements without neglecting the simplifying assumption of separate spatial correlation at the two link ends. While such a model is employed in a typical wireless communication system design, it could be possible to build useful model parameters, which leads to adaptive system structures.

In the dissertation [15], the author states two novel correlative channel models which are based on approximations of $\mathbf{R}_{H,\ell}$. According to the

concept of the vector modes in his thesis, the first channel model can be defined. Another popular version is based on the novel concept, named structured modes. The last model is presented in many literatures, and it will be viewed as the Weichselberger model in the following derivations.

Since the Weichselberger model takes into account the joint spatial structure and describes the MIMO propagation channel using the one-sided correlation matrices, it is a novel MIMO propagation channel model. The eigenbases of the one-side correlation matrices are the same as in the Kronecker model and they are coupled with coupling matrix.

Consider the narrowband channel matrix $\mathbf{H}_{\ell,n}$, the Eigen-value decomposition(EVD) of the correlation matrix $\mathbf{R}_{H,\ell}$ is generated because it is PSD Hermitian symmetric and presented through the following equation.

$$\begin{aligned}\mathbf{R}_{H,\ell} &= \sum_{i=1}^{KM} \lambda_{H,i}\mathbf{u}_{H,i}\mathbf{u}_{H,i}^{H} \\ &= \mathbf{U}_{H,\ell}\mathbf{\Lambda}_{H,\ell}\mathbf{U}_{H,\ell}^{H}\end{aligned} \tag{3.7}$$

where $\mathbf{U}_{H,\ell}$ is the spatial eigenbases of the full channel correlation matrix, which is unitary matrix, and $\Lambda_{H,\ell}$ is diagonal matrix composed with the eigen values of $\mathbf{R}_{H,\ell}$.

As stated in the Kronecker model, the one-sided correlation matrices are Hermitian, so it can be decomposed by using EVD, formulated as

$$\begin{aligned}\mathbf{R}_{\mathrm{Rx},\ell} &= \sum_{k=1}^{K} \lambda_{\mathrm{Rx},k}\mathbf{u}_{\mathrm{Rx},k}\mathbf{u}_{\mathrm{Rx},k}^{H} \\ &= \mathbf{U}_{\mathrm{Rx},\ell}\mathbf{\Lambda}_{\mathrm{Rx},\ell}\mathbf{U}_{\mathrm{Rx},\ell}^{H}\end{aligned} \tag{3.8}$$

$$\begin{aligned}\mathbf{R}_{\mathrm{Tx},\ell} &= \sum_{m=1}^{M} \lambda_{\mathrm{Tx},m}\mathbf{u}_{Tx,m}\mathbf{u}_{\mathrm{Tx},m}^{H} \\ &= \mathbf{U}_{\mathrm{Tx},\ell}\mathbf{\Lambda}_{\mathrm{Tx},\ell}\mathbf{U}_{\mathrm{Tx},\ell}^{H}\end{aligned} \tag{3.9}$$

where $\lambda_{\mathrm{Rx},k}$ and $\lambda_{\mathrm{Tx},m}$ are the eigenvalues for the receive-correlation matrix and the transmit-correlation matrix, $\mathbf{u}_{\mathrm{Rx},k}$ and $\mathbf{u}_{\mathrm{Tx},m}$ are the receive and transit eigenvectors, and $\mathbf{U}_{\mathrm{Rx},\ell}$ and $\mathbf{U}_{\mathrm{Tx},\ell}$ are the receive and transmit eigenbases, respectively. Also, $\mathbf{u}_{\mathrm{Rx},k}$ and $\mathbf{u}_{\mathrm{Tx},m}$ are referred to as the one-sided eigenvectors, $\mathbf{U}_{\mathrm{Rx},\ell}$ and $\mathbf{U}_{\mathrm{Tx},\ell}$ are called as the one-sided eigenbases.

Given the eigenbases of the full channel correlation matrix, it can be recast in terms of the eigenbasis at the receiver and transmitter as follows:

$$\mathbf{U}_{H,\ell} = \mathbf{U}_{\mathrm{Rx},\ell} \otimes \mathbf{U}_{\mathrm{Tx},\ell} \tag{3.10}$$

Using the relation in 3.10, the Weicheselberger model can be reformulated for each subcarrier ℓ and given below:

$$\mathbf{H}_{\text{Weich},\ell} = \mathbf{U}_{\text{Rx},\ell}(\tilde{\mathbf{\Omega}}_\ell \odot \mathbf{G}_\ell)\mathbf{U}_{\text{Tx},\ell}^T \tag{3.11}$$

where $\mathbf{G}_\ell \in \mathcal{C}^{\mathcal{K}\times\mathcal{M}}$ is the i.i.d matrix with zero-mean and unit variance, the operator $\odot$ represents the element-wise product of two matrixes (or the Hadamard product), and $\mathbf{U}_{\text{Rx},\ell}$ and $\mathbf{U}_{\text{Tx},\ell}$ are complex unitary matrices including the eigenvectors of $\mathbf{R}_{\text{Rx},\ell}$ and $\mathbf{R}_{\text{Tx},\ell}$, respectively, that is,

$$\mathbf{U}_{\text{Rx},\ell} = [\mathbf{u}_{\text{Rx},1} \cdots \mathbf{u}_{\text{Rx},K}] \tag{3.12}$$

$$\mathbf{U}_{\text{Tx},\ell} = [\mathbf{u}_{\text{Tx},1} \cdots \mathbf{u}_{\text{Tx},M}] \tag{3.13}$$

Also, $\tilde{\mathbf{\Omega}}_\ell$ denotes the element-wise square root of the power coupling matrix $\mathbf{\Omega}_\ell$ obtained by:

$$\mathbf{\Omega}_\ell = \begin{pmatrix} \omega_{11} & \cdots & \omega_{1M} \\ \vdots & \ddots & \vdots \\ \omega_{K1} & \cdots & \omega_{KM} \end{pmatrix}$$

where ω_{km} is defined as the coupling coefficient and given through the following equation:

$$\begin{aligned} \omega_{km} &= E\{\|\mathbf{u}_{\text{Rx},k}^H \mathbf{H} \mathbf{u}_{\text{Tx},m}^*\|^2\} \\ &= E\{[(\mathbf{u}_{\text{Tx},m} \otimes \mathbf{u}_{\text{Rx},k})^H \text{vec}(\mathbf{H})]^H [(\mathbf{u}_{\text{Tx},m} \otimes \mathbf{u}_{\text{Rx},k})^H \text{vec}(\mathbf{H})]\} \\ &= (\mathbf{u}_{\text{Tx},m} \otimes \mathbf{u}_{\text{Rx},k})^H \mathbf{R}_H (\mathbf{u}_{\text{Tx},m} \otimes \mathbf{u}_{\text{Rx},k}) \end{aligned} \tag{3.14}$$

The power coupling matrix $\mathbf{\Omega}_\ell$ refers to the coupling coefficients that are defined as the average power coupled between an eigenvector at the receive side and an eigenvector at the transmit side. Therefore, $\mathbf{\Omega}_\ell$ is dependent on the environment and can reflect the scattering structure of the environment.

It is easy to achieve the parameters of the Weicheselberger modle by compute the EVD of the one-sided correlation matrices. Furthermore, the structure of $\mathbf{\Omega}_\ell$ can let us know more about the spatial structure of the channel. However, the main disadvantage of the Weicheselberger versus Kronecker model is also from the $\mathbf{\Omega}_\ell$ in term of the number of the parameters, since the more parameters are required to express it except for the eigenbases of the one-sided correlation matrices.

In general, despite the main disadvantage of the Weicheselberger model, it has been shown to support a more accurate MIMO propagation channel by using real-life data [15]. Using the Equation 3.11, the Weicheselberger model can be obtained based on the real data from the massive MIMO measurement. After constructing the correlative channel models, we compare the performance of the Weicheselberger versus Kronecker models. The evaluation and comparison for models will be given in the later chapter.

3.2 Validation Metrics

In this section, a few metrics used in the literature are employed to verify the performance of channel models. Each metric is provided an interpretation and examines a different aspect of the model. Thesis metrics are used in comparing the correlative models' ability to predict the measured channels for our work, which give us absolute references.

3.2.1 System Model

Consider the uplink transmission of a single-cell MU-MIMO channel system with M antennas at the BS and K single-antenna users ($K \leq M$). Orthogonal frequency division multiplexing(OFDM) with L subcarriers is used to reduce the correlation in the user sides. The communication between the BS and the users takes place in the subcarriers L and snapshots N. The channel input-output relationship is given at subcarrier ℓ and snapshot n, that is

$$\mathbf{y}_{\ell,n} = \sqrt{\frac{P}{M}}\mathbf{H}_{\ell,n}\mathbf{x}_{\ell,n} + \mathbf{w}_{\ell,n} \tag{3.15}$$

Where $\mathbf{H}_{\ell,n} \in \mathcal{C}^{\mathcal{M}\times K}$ represents the channel matrix between the BS and the users; $\mathbf{y}_{\ell,n} \in \mathcal{C}^{\mathcal{M}\times 1}$ and $\mathbf{x}_{\ell,n} \in \mathcal{C}^{\mathcal{K}\times 1}$ are the output and input vectors, respectively and $\mathbf{w}_{\ell,n} \in \mathcal{C}^{\mathcal{M}\times 1}$ is the noise vector at the receiver whose elements are i.i.d with zero mean and unit variance; P is the total transmit power and $\frac{P}{M}$ refers to the average transmitted power.

3.2.2 Normalization

With the Equation 3.15 proposed, it is easy to achieve the instantaneous signal to noise ratio (SNR) per receive antenna, which results in averaged over all receive antennas, that is given by

$$\rho = \frac{P}{\sigma_w^2}\frac{\|\mathbf{H}_{\ell,n}\|_F^2}{KM} \tag{3.16}$$

where σ_w^2 means the variance of the noise vector. However, it is assumed as 1 in our system in order to simplify the model.

For our simulation, the different MIMO systems and configurations such as M = 128, 64 and 32 are used. Therefore, it is required to ensure a fair comparison of the capacity performance for the different configurations, and since the total power P has been fixed, the solving strategy is to consider the same receive SNR, as below:

Considering the measured channel matrix $\mathbf{H}_{\ell,n}$ taken over all N measurement snapshots and L subcarriers, the normalized channel matrix can be expressed as

$$\mathbf{H}_{\ell,n}^{\text{norm}} = \sqrt{\frac{KMLN}{\sum_{n=1}^{N}\sum_{l=1}^{L}\|\mathbf{H}_{\ell,n}^{\text{meas}}\|_F^2}}\mathbf{H}_{\ell,n}^{\text{meas}} \tag{3.17}$$

It is easily followed that

$$\frac{1}{L}\sum_{\ell=1}^{L}\frac{1}{N}\sum_{n=1}^{N}\|\mathbf{H}_{n,\ell}^{\text{norm}}\|_F^2 = KM \tag{3.18}$$

In the Equation 3.17, the average of the Frobenius norm of the channel snapshots and subcarriers are fixed, and the normalization can preserves the relative difference in the channel power over time-frequency resources, but keep the average of the SNR at $\frac{P}{\sigma_w^2}$ (σ_w^2=1). These normalization can satisfy a fair comparison, because the obtained average SNR from normalization is equivalent to the average SNR of a SISO system with the same power and noise power.

3.2.3 Uplink Capacity for MU-MIMO

For the uplink transmission of the MU-MIMO system, we assume the CSI is unknown by the transmitter, all users have the same transmit power allocation. The uplink capacity at subcarrier ℓ is obtained in the unit of bps/Hz as [22]

$$\mathbf{C}_{\text{uplink},\ell} = \log_2\det(\mathbf{I}_M + \frac{E_s}{MN_0}\mathbf{H}_\ell^H\mathbf{H}_\ell) \tag{3.19}$$

where $\mathbf{I}_M$ is the identity matrix and $\mathbf{H}_\ell$ is the channel response matrix at subcarrier ℓ. The average SNR, which denoted by $\frac{E_s}{MN_0}$, is decreased with the increasing M thus the array gain can be obtained.

3.2.4 Zero-Forcing Pre-Coding Sum-Rate

The sum-rate of the MU-MIMO uplink can be achieved by the ZF pre-coding scheme, which is one of the most popular linear pre-coding techniques, aiming to remove the ISI (Inter-Symbol Interference). The ZF pre-coder can be written as

$$\mathbf{W}_{\text{ZF}} = (\mathbf{H}^*\mathbf{H}^T)^{-1}\mathbf{H}^* \tag{3.20}$$

By computing $\mathbf{W}_{\mathrm{ZF}}$ into the the signal model, the sum-rate capacity of ZF pre-coding becomes

$$\mathbf{C}_{\mathrm{ZF},\ell} = \sum_{i=1}^{K} \log_2(1 + \frac{\frac{E_s}{M}}{N_0[(\mathbf{H}_\ell^* \mathbf{H}_\ell^T)^{-1}]_{ii}}) \tag{3.21}$$

where $\frac{E_s}{M}$ is the signal power of ith user, and $N_0[(\mathbf{H}_\ell^* \mathbf{H}_\ell^T)^{-1}]_{ii}$ is the noise power of ith user.

3.2.5 Singular Value Spread

This section presents another performance metric to analysis the massive MIMO radio channel, singular value spread (also known as the condition number). The channel matrix $\mathbf{H}$ has a singular value decomposition:

$$\mathbf{H} = \mathbf{U}\mathbf{\Sigma}\mathbf{V}^H \tag{3.22}$$

where $\mathbf{U} \in \mathcal{C}^{\mathcal{K}\times\mathcal{K}}$ and $\mathbf{V} \in \mathcal{C}^{\mathcal{M}\times\mathcal{M}}$ are unitary matrices. The diagonal matrix $\Sigma \in \mathcal{C}^{\mathcal{K}\times\mathcal{M}}$ is composed by the singular values $\sigma_1, \sigma_2, \cdots, \sigma_k$, the singular value spread κ is defined as:

$$\kappa = \frac{\sigma_{\max}}{\sigma_{\min}} \tag{3.23}$$

where σ_{max} and σ_{min} are the maximal and minimal singular values, respectively. The κ $(1 \leq \kappa \leq \infty)$ is the ratio between $\sigma_{\max}$ and $\sigma_{\min}$, where $\kappa = 1$ indicates a orthogonal channel matrix, otherwise a large κ shows that at least two rows of the $\mathbf{H}$ are similar, which means at least one of the K users will not be served.

Chapter 4

Validation of Correlative Models

In the previous chapter, we have introduced the four measurement campaigns in order to support the measured data and discussed a few metrics commonly used to validate the performance of channel models. In this chapter, the selected measurement scenarios were collected in very different environments, using two large antenna arrays whose specifications differ.

In order to determine the correlative models' usefulness in massive MIMO, three validation metrics uplink capacity, ZF sum-rate and singular value are shown in the below sections for the selected measurement scenarios. The validation metrics give an accuracy with which a model characterizes the massive MIMO channels, thus, we can use them to verify the correlative models. Furthermore, we compare the metrics achieved in the measured channels with those achieved in the correlative models according to different aspects, such as the propagation condition, i.e., LOS versus NLOS; propagation environment, i.e., indoor versus outdoor; the environment at user side, i.e., crowded versus non-crowded; and different BS locations.

4.1 Linear Array

This section introduces the validation results of the correlative models, when chosen scenarios are gathered in the first measurement campaign ("ULA with 5 virtual users"). For the measured channels and the correlative models, the three validation metrics are shown on the order of 5, 32, 64 and 128 antennas equipped at the BS.

4.1.1 Selection of Antennas

Different number of antennas at the BS gives different channel performance. Here, we describe the method of antenna selection in detail and try to cover

all antennas on the array:

1. M = 128: All antennas on the array are used.

2. M = 64: The adjacent antenna sliding window with 64 antennas is selected to slide from the first antenna to the final one, when considering the ULA. After that, there are 65 sliding windows for our selection in total. We do a simulation for each sliding window, so the 65 simulation results are achieved to calculate the uplink capacity, ZF sum-rate and singular value, then the calculated parameters are averaged over different simulations.

3. M = 32 and 5: Except for the sliding window size is 32 and 5 antennas, respectively, the same method is used as M =64.

4.1.2 ULA with 5 Virtual Users

To observe the performance of the correlative models in LOS and NLOS propagation conditions, the measured data gathered in the following two scenarios are used.

- The first scenario occurs in a LOS outdoor environment. The five users are close to each other at MS 2, whereas the BS remains fixed. Details on the position information can be found in the Figure 2.2. In order to have the strongest LOS characteristic, we choose this scenario to be investigated.

- The second scenario is the same outdoor environment as the first scenario, however, the close five users are at MS 5 and communicate with BS in a NLOS condition. This scenario is used because there are rich scatterers between the user and the BS.

LOS Scenario

Figure 4.1 shows both the uplink capacity and the ZF sum-rate as a function of E_s/N_0 (-10 to 10 dB) for different antenna deployments, when considering the Kronecker model in LOS scenario. It can be known from the figure that the uplink capacity for the measured channels and the Kronecker model increases as E_s/N_0 increases for 5, 32, 64 and 128 antennas, respectively. Furthermore, it also becomes larger, when increasing the number of BS antennas. For the ZF sum-rate, it goes to larger value as a function of the number of BS antennas for the measured channels. However, for the Kronecker model, it keeps in 0 [bps/Hz] expect for M = 128.

It is easy to observe that there is a long rates gap between the measured channels and the Kronecker model for 32, 64 and 128 antennas, when considering the uplink capacity and the ZF sum-rate. Moreover, the gaps become large, when the BS has more antennas. But, the gaps are not too bad for M = 5, as comparing with larger number of antennas at BS.

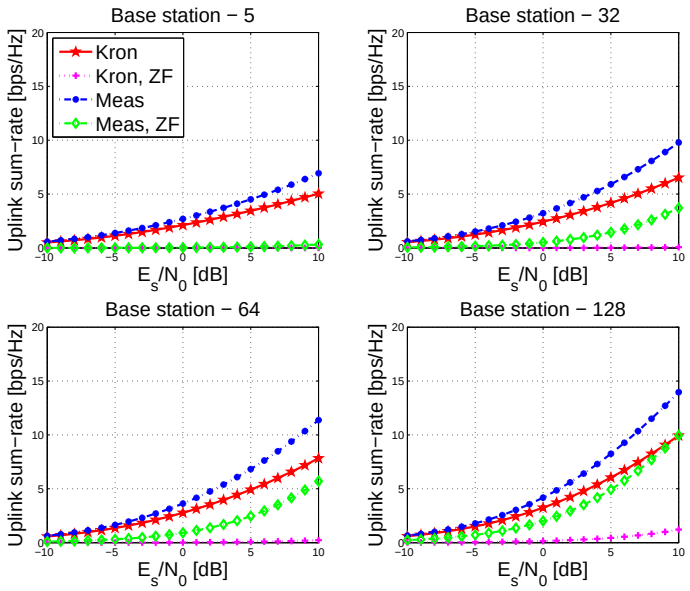

Figure 4.1: Validation of the Kronecker model. Measurement campaign: ULA with 5 virtual users; User location: MS 2; Propagation condition: LOS.

In Figure 4.2, we display the cumulative distribution functions (CDFs) of singular values for the measured channels and the Kronecker model in LOS scenario. The blue lines in the figure give the singular values in the measured channels, and the median of singular value spreads are 20 dB, 12 dB, 10 dB and 7 dB for 5, 32, 64 and 128 BS antennas. The red lines in the figure announce the singular values of the Kronecker model, which show that the median of singular value spreads are 37 dB, 23 dB, 21 dB and 16 dB. The median values for both the measured channels and the Kronecker model become smaller, when having more antennas at BS. The median values in the Kronecker model are higher than those in the measured channel and reduce significantly, it leads to a worse channel orthogonality for the users.

Using the same measured data, the Weichselberger model can be generated, thus, the performances of the measured channels give the same as shown in Figure 4.1. Here, we are primarily interested in viewing the generated model's performance by considering the uplink capacity and the ZF

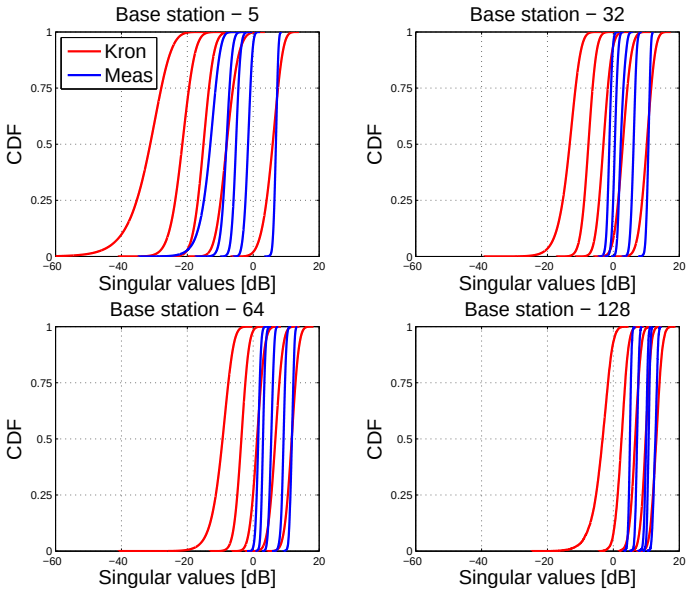

Figure 4.2: CDFs of singular values for the 5 users in measured and the Kronecker model channel. Measurement campaign: ULA with 5 virtual users; User location: MS 2; Propagation condition: LOS.

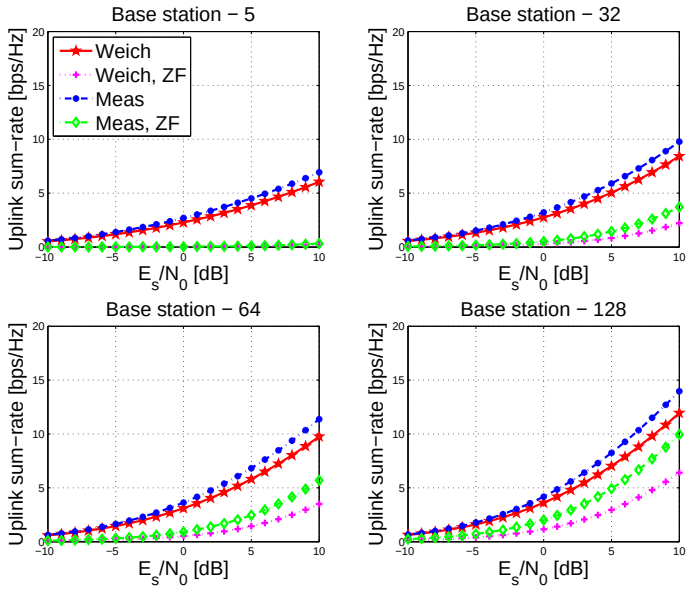

Figure 4.3: Validation of the Weichselberger model. Measurement campaign: ULA with 5 virtual users; User location: MS 2; Propagation condition: LOS.

sum-rate. Figure 4.3 illustrates the gaps between the measured channels and the Weichselberger model become smaller for both the uplink capacity and the ZF sum-rate, when comparing with the gaps achieved in the Figure 4.1. Once more, the figure shows the gaps for M = 5 is smaller than others (M = 32, 64 and 128).

We now study the CDFs of singular values for the Weichselberger model, as shown in Figure 4.4. It can be seen from the figure that the median of singular value spreads for the measured channels are the same as shown in Figure 4.2, and for the Weichselberger model are 20 dB, 13 dB, 11 dB and 9 dB based on the different antenna configuration.

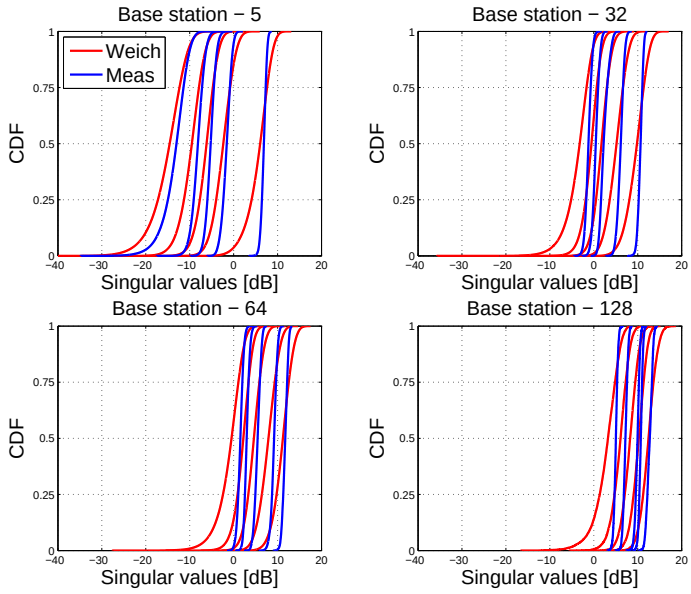

Figure 4.4: CDFs of singular values for the 5 users in measured and the Weichselberger model channel. Measurement campaign: ULA with 5 virtual users; User location: MS 2; Propagation condition: LOS.

Therefore, for this selected LOS scenario, when comparing the performance metrics between the measured channels and the correlative models, we can observe that the uplink capacity obtained by the Weichselberger model is higher than that achieved in the Kronecker model, for 5, 32, 64 and 128 antennas, respectively. This characteristic also can be observed for the ZF sum-rate, except for 5 antennas at BS.

NLOS Scenario

Comparing with the LOS scenario above, the validation results are collected in the NLOS scenario below. From the Figure 4.5, it is easy to observe that when considering the measured channels and the Kronecker model, both the uplink capacity and the ZF sum-rate achieved in NLOS scenario are greater than those achieved in LOS scenario (see Figure 4.1), since rich scatterers within NLOS scenario allow better spatial separation of user signals.

Notice that the gap between the uplink capacity and the ZF sum-rate for the measured channel becomes smaller, as increasing the number of BS antenna. The reason for this is that ZF pre-coder consumes power to remove ISI, however, the consumption decreases as the number of BS antenna increases. That leads to the resulting ZF sum-rate goes to the uplink capacity. Despite the environment is improved, both the uplink capacity and the ZF sum-rate obtained by the Kronecker model underestimate those achieved in the measured channels.

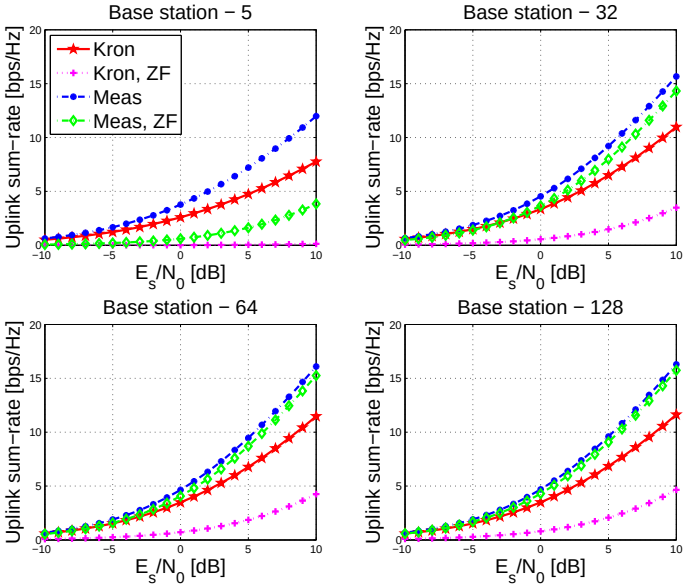

Figure 4.5: Validation of the Kronecker model. Measurement campaign: ULA with 5 virtual users; User location: MS 5; Propagation condition: NLOS.

The CDFs of singular values shown in Figure 4.6 is used to check if the Kronecker model can represent the measured channel. For this NLOS scenario, the singular values become smaller than the LOS scenario for the measured channels and the Kronecker model; and the median of the singular value spreads display 12 dB, 4 dB, 3 dB and 2 dB for the measured

channels, 24 dB, 12 dB, 11.5 dB and 11 dB for the Weichselberger model, for all cases of 5, 32, 64 and 128 antennas. Obviously the median values of the model are larger than the measured channels, so it is not a good model to represent the measured channels.

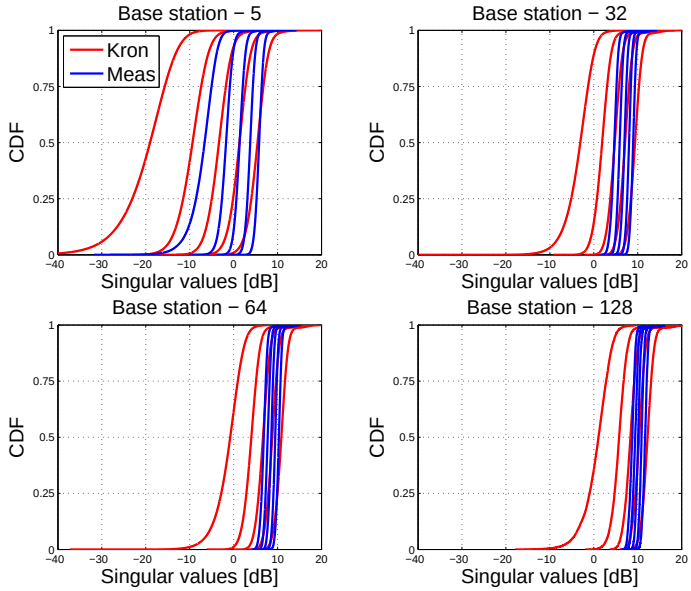

Figure 4.6: CDFs of singular values for the 5 users in measured and the Kronecker model channel. Measurement campaign: ULA with 5 virtual users; User location: MS 5; Propagation condition: NLOS.

We now use measured data from NLOS scenario to generate the Weichselberger model and describe its uplink capacity and ZF sum-rate when using different number of antennas, as shown in Figure 4.7. The Weichselberger model supports higher uplink capacity and ZF sum-rate than the Kronecker model for 5, 32, 64 and 128 antennas in this NLOS scenario, when comparing with Figure 4.5. Because of this reason, the Weichselberger model is closer to the measured model than the Kronecker model.

In Figure 4.8, the median of singular value spreads are 13 dB, 7 dB, 6.5 dB and 6 dB for equipping 5, 32, 64 and 128 antennas at the BS, respectively. Compare the CDF curves of singular values between the measured channels and the Weichselberger model, both singular values are close, however, they also give some difference. Singular value spreads can reflect the benefits of complex propagation. Both the measured channels and the Weichselberger model have smaller singular value spreads. That indicates a much better user channel orthogonality in the measured channels and the model channels.

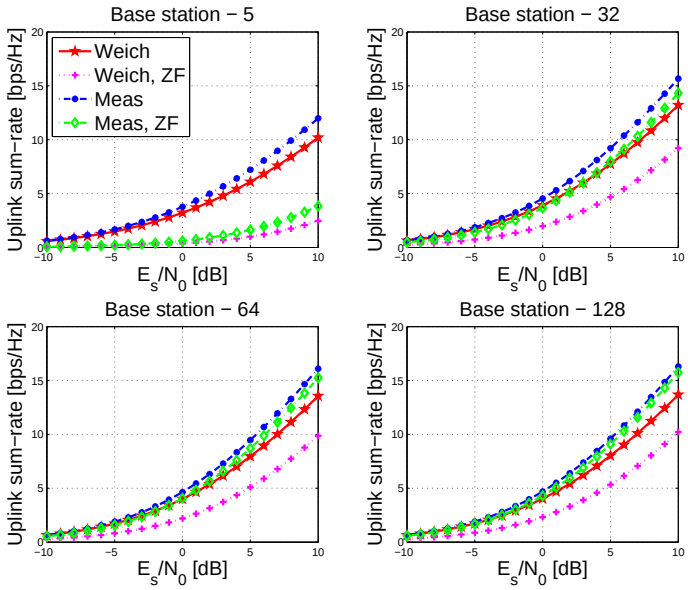

Figure 4.7: Validation of the Weichselberger model. Measurement campaign: ULA with 5 virtual users; User location: MS 5; Propagation condition: NLOS.

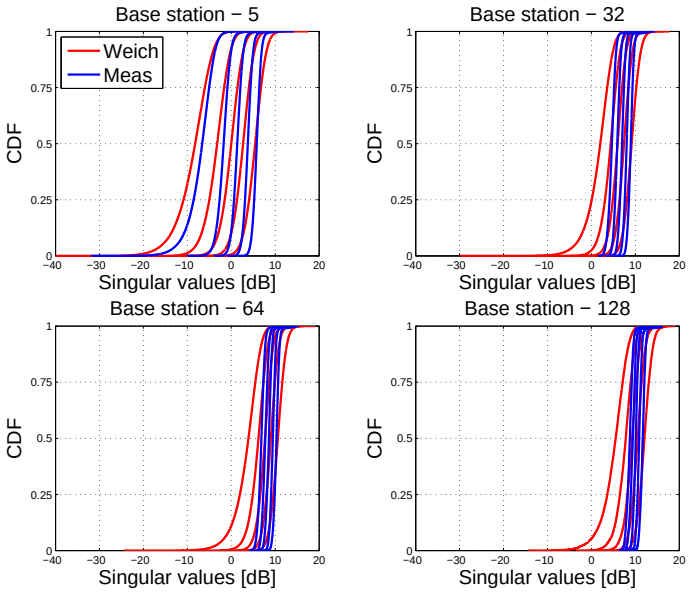

Figure 4.8: CDFs of singular values for the 5 users in measured and the Weichselberger model channel. Measurement campaign: ULA with 5 virtual users; User location: MS 5; Propagation condition: NLOS.

Summarizing, we find that the Weichselberger model is more closer to the measured channels than the Kronecker model, when considering the LOS scenario and NLOS scenario, respectively. That is due to the separability assumption for the Kronecker model that scatterers at both sides can not be coupled. Furthermore, when considering the Kronecker model and the Weichselberger model, respectively, NLOS scenario with rich scatterers can bring the better benefits than the LOS scenario, since scatterers in the environment can support strong decorrelation effect to the channel.

4.2 Cylindrical Array

In order to compare with linear array, the chosen scenarios in this section are gathered in the measurement campaigns performed with UCA at BS, which are "UCA with 5 virtual users", "UCA with 9 synchronized users - outdoor", "UCA with 9 synchronized users - indoor". With the order of 5 (or 9), 32, 64 and 128 antennas equipped at BS, the three validation metrics are shown in the following, the antenna selection method will also be presented.

4.2.1 Selection of Antennas

Here, the antenna selection of UCA is introduced, and it will be used for all validation results of UCA:

1. M = 128: All antenna ports are used.
2. M = 64: We randomly choose two rings from the four rings of the UCA, thus, the 6 possible selections are got to do simulations and then average them.
3. M = 32: We select one ring among the four rings at one time and give 4 selection methods. Using the 4 selections, four simulation results are achieved and then also average them.
4. M= 5 (or 9): For each ring of the four rings, the 5 (or 9) antenna ports are evenly spaced by 6-7 (or 3-4) antenna ports. After that, the spaced 5 (or 9) antenna ports start circulating in a clock wise direction. Since each ring has 32 antenna ports, 6 (or 3) possible selections are given for each ring. Thus, 24 (or 12) selection ways are selected to consider the 128 ports. Finally, we can simulate the sum-rates for each selection way and calculate the mean value of them.

4.2.2 UCA with 5 Virtual Users

In this subsection, the measured data is from the second measurement campaign. It is important to know that the measured data is from the first half of the 40 positions, since the user travels long distance over the positions and the environment has changed. As mentioned in the section 4.1, validation results of the two correlative model are based on the same scenario as before in order to compare the performance of the UCA and ULA.

LOS Scenario

Given the Figure 4.9, a good experimental result has been provided. It is clear from the simulation results that for the measured channels and the Kronecker model, the uplink capacity and the ZF sum-rate stay the same for different antenna deployments at BS. However, when using more antennas at BS (>5), both the uplink capacity and the ZF sum-rate increase neglectfully.

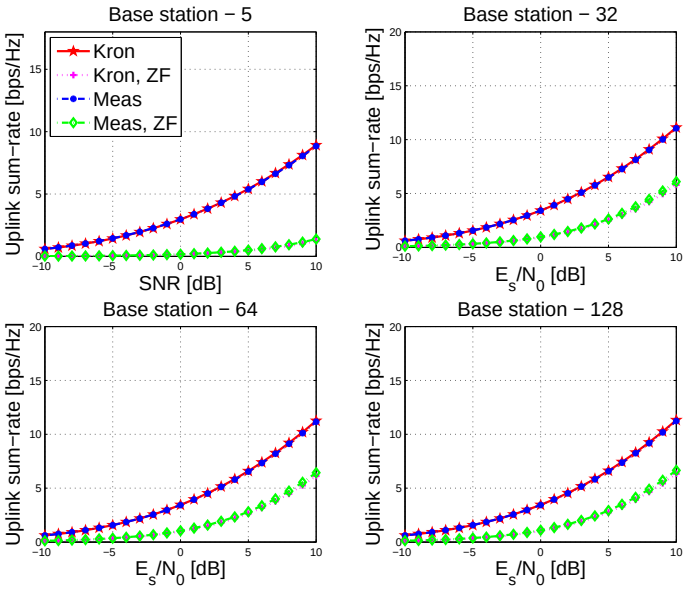

Figure 4.9: Validation of the Kronecker model. Measurement campaign: UCA with 5 virtual users; User location: MS 2; Propagation condition: LOS.

Moreover, as compared to Figure 4.1, we see that with UCA, the uplink capacity and the ZF sum-rate are improved for 5, 32, and 64 antennas, however, when BS has 128 antennas, both the uplink capacity and the ZF sum-rate for the measured channels reduce.

Consider the CDFs of singular values in Figure 4.10, the median of singular value spreads for 5, 32, 64 and 128 antennas are 16 dB, 10 dB, 9.5 dB and 9 dB for the measured channel. For the Kronecker model, they are 16 dB, 10 dB, 9.9 dB and 9.5 dB. It seems to be a negligible between the measured channels and the Kronecker model. Furthermore, the CDF curves just have unsubstantial upper tails as M exceeds the number of users (K = 5).

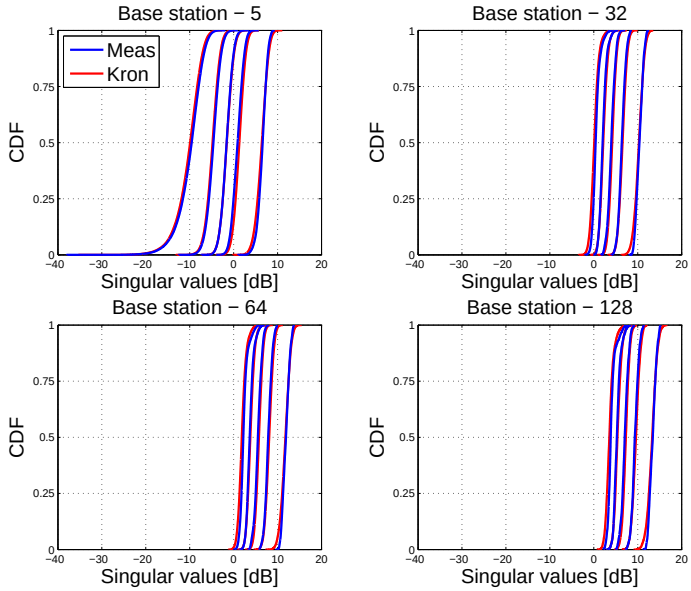

Figure 4.10: CDFs of singular values for the 5 users in measured and the Kronecker model channel. Measurement campaign: UCA with 5 virtual users; User location: MS 2; Propagation condition: LOS.

Here, the Weichselberger model is generated by using the same LOS scenario with the above Kronecker model. Thus, the performance metrics of the measured channels show the same characteristics, as given in the above Kronecker model.

From the Figure 4.11, UCA can do better than ULA, as compared to Figure 4.3. Note that the uplink capacity and the ZF sum-rate achieved in the Weichselberger model overestimate those achieved in the measured channel. Although the half of the measured data is used, the user still moves up to 10m. The distance leads to the slightest mistake, so our simulation can be accepted.

Figure 4.12 shows the CDFs of singular values for the measured channel and the Weichselberger model. By surveying the figure, the median of singular value spreads obtained in the Weichselberger model are 15.5 dB, 9

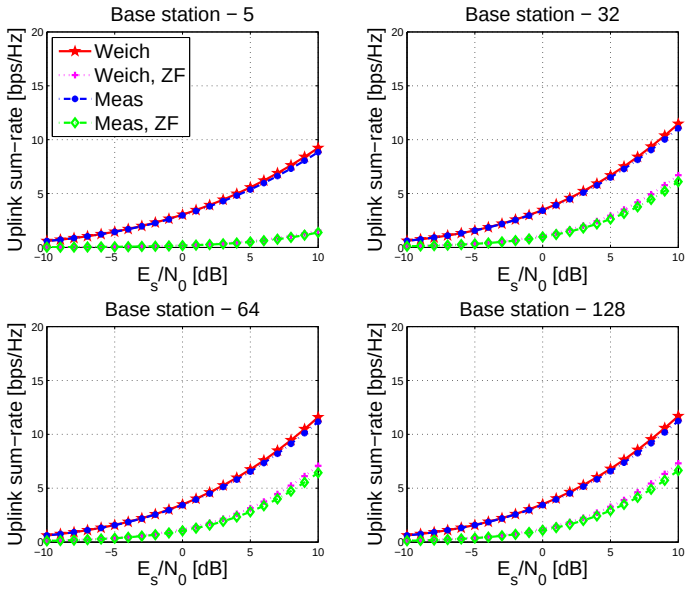

Figure 4.11: Validation of the Weichselberger model. Measurement campaign: UCA with 5 virtual users; User location: MS 2; Propagation condition: LOS.

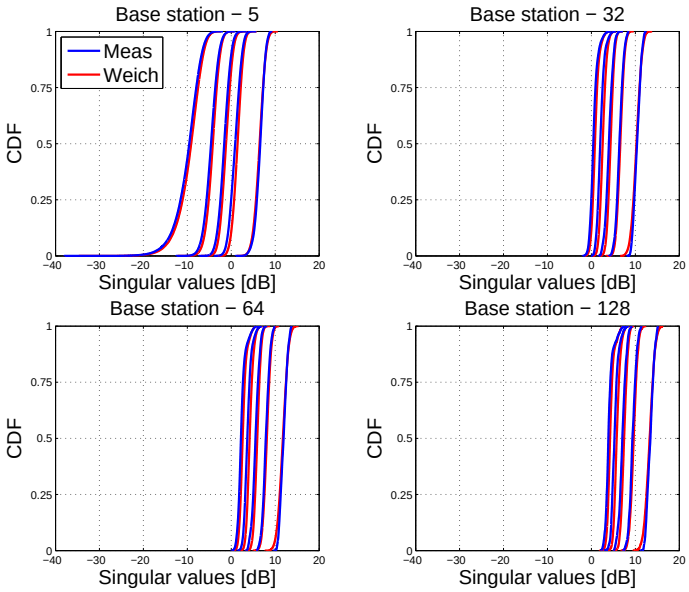

Figure 4.12: CDFs of singular values for the 5 users in measured and the Weichselberger model channel. Measurement campaign: UCA with 5 virtual users; User location: MS 2; Propagation condition: LOS.

dB, 9 dB and 8.9 dB for different antenna deployment. When M is larger than 5, CDF curves become more stable.

In this LOS scenario, the contribution of the correlative models to the measured channels from massive MIMO can be viewed as sameness. The Weichselberger model has been shown to be accurate than the Kronecker model in the literature, however, it does not be supported, when considering massive MIMO performed with UCA at BS.

NLOS Scenario

In contrast to the LOS scenario above, validation results of correlative models for the NLOS scenario will be given in the next paragraphs.

From Figure 4.13, it is clear that both the uplink capacity and ZF sum-rate achieved in NLOS scenario are always higher than those achieved in LOS scenario for the measured channels and the Kronecker model, when compared with the Figure 4.9. It is worth mentioning that the improvement in the ZF sum-rate if using more antenna (>5). That is because as the number of the antenna increasing, ZF consumes less power, which leads to the ZF sum-rate become larger and close to the measured channels.

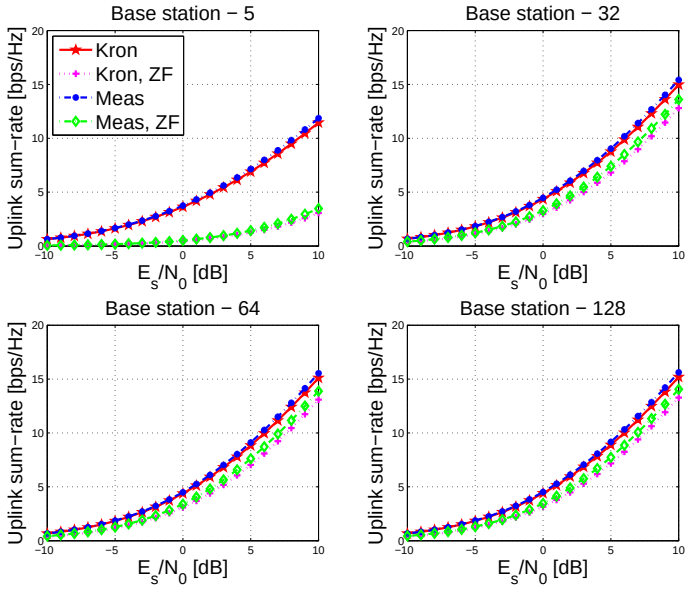

Figure 4.13: Validation of the Kronecker model. Measurement campaign: UCA with 5 virtual users; User location: MS 5; Propagation condition: NLOS

Consider the CDFs of singular values in this NLOS scenario, as shown in Figure 4.14. The median of singular value spreads are 13 dB, 5 dB, 4.7

dB and 4.5 dB for the measured channels when equipping 5, 32, 64 and 128 antennas at BS. Furthermore, the median values for the Kronecker model (13 dB, 5.5 dB, 5 dB and 5 dB) also can be caught for different antenna number in the figure. The median values in this scenario for both the measured channels and the Kronecker model are smaller than the median values achieved in the LOS conditions (see Figure 4.10). Moreover, it can be observed that the lines become tighter as the antenna increases, that let singular value spreads become much more stable.

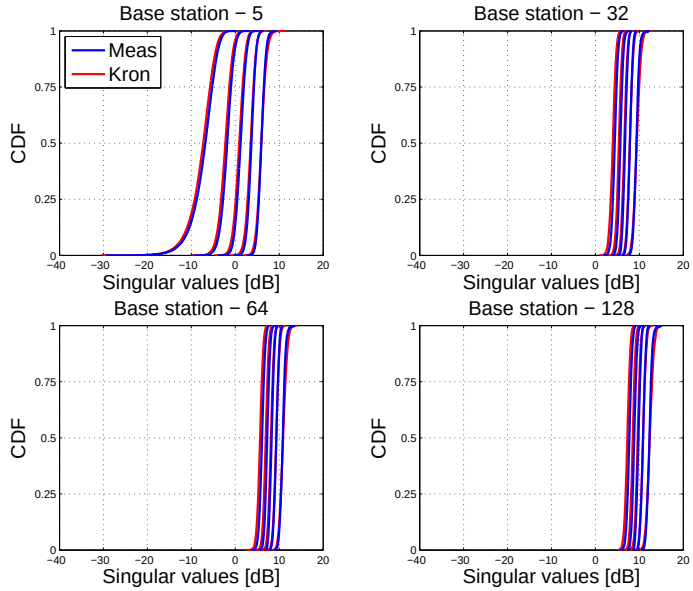

Figure 4.14: CDFs of singular values for the 5 users in measured and the Kronecker model channel. Measurement campaign: UCA with 5 virtual users; User location: MS 5; Propagation condition: NLOS.

Using the measured data from the NLOS scenario, the Weichselberger model is generated. After that, the metrics are computed. Observing Figure 4.15 and Figure 4.13, it is difficult to distinguish both figures. That can prove that we can not determine which model is more accurate.

As can be seen in Figure 4.16, singular values for the Weichselber model give the same characteristic as the Kronecker model, when compared to those in Figure 4.14.

When considering the NLOS scenario, validation metrics created by the Kronecker model give the same variation as shown in the Weichselberger model. Thus, the Weichselberger model is not more accurate than the Kronecker model.

Clearly, compared to the section 4.1, UCA shows good performance

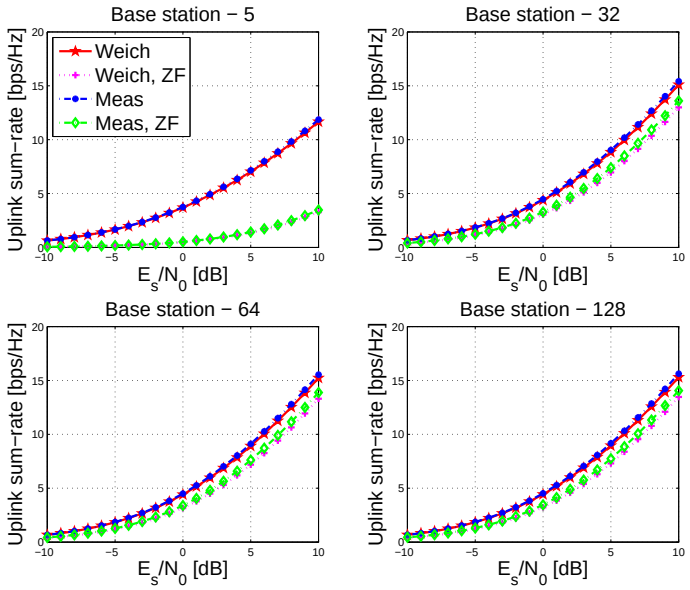

Figure 4.15: Validation of the Weichselberger model. Measurement campaign: UCA with 5 virtual users; User location: MS 5; Propagation condition: NLOS

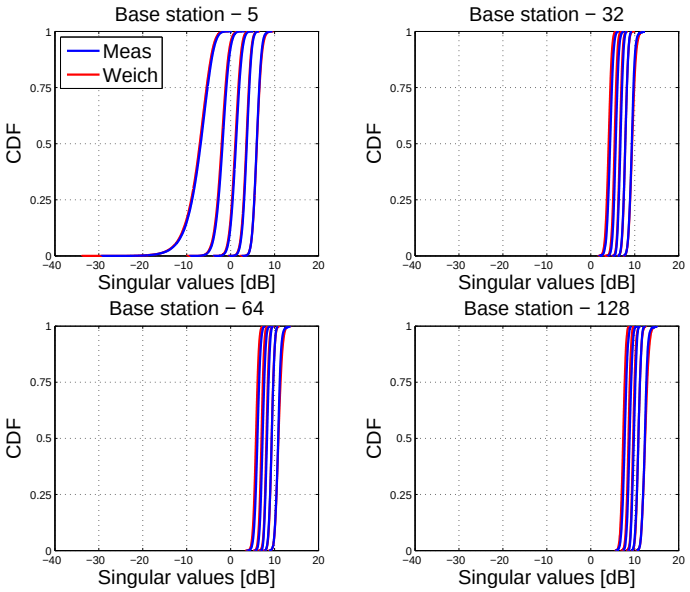

Figure 4.16: CDFs of singular values for the 5 users in measured and the Weichselberger model channel. Measurement campaign: UCA with 5 virtual users; User location: MS 5; Propagation condition: NLOS.

than ULA. On the other hand, it is very likely that the two correlative models are great models to model the measured channel by the validation metrics, when considering the measured data from the second measurement campaign. And in the future, it is really needed to do more research for the two correlative models.

However, for this measurement campaign, we measured the 40 positions with a inter-spacing of 0.5m, that results in the variation of the environment. To reduce the changes of the environment, we remove the last half of the measured data for our simulation, however, that still leads to some challenges.

4.2.3 UCA with 9 Synchronized Users - Outdoor

It is important the fact that the third measurement campaign employs 9 simultaneous real users to communicate with the UCA BS. Thus, it is obvious that the correlative models modelled in this measurement campaign could have significant differences relative to the measurement campaign employed 5 virtual users.

As simulated in the first two measurement campaigns, the LOS scenario and the NLOS scenario were considered. We study the same two kinds of scenarios for this campaign, and except for the LOS condition and the NLOS condition, we also consider a heavy crowed condition with 10-12 persons. The measurement sites used in this subsection has been shown in Figure 2.3a.

The investigated scenarios are:

- The first used scenario is measured at MS 1, as shown in Figure 2.3a, and MS 1 has LOS condition. Furthermore, the 9 active users are crowded by another 10 to 12 persons or not.
- The another scenario is performed at MS 3, that has NLOS condition. The 9 active users with the crowd and without the crowd also be observed.

LOS Scenarios

Figure 4.17 shows the uplink capacity and the ZF sum-rate between the measured channels and the Kronecker model. For 9, 32, 64, and 128 antennas, respectively, the uplink capacity and the ZF sum-rate for both the measured channels and the Kronecker model go to a high level, as compared to Figure 4.9. The reason is the more the users we employ, the better the sum-rate, according to the Shannon theorem.

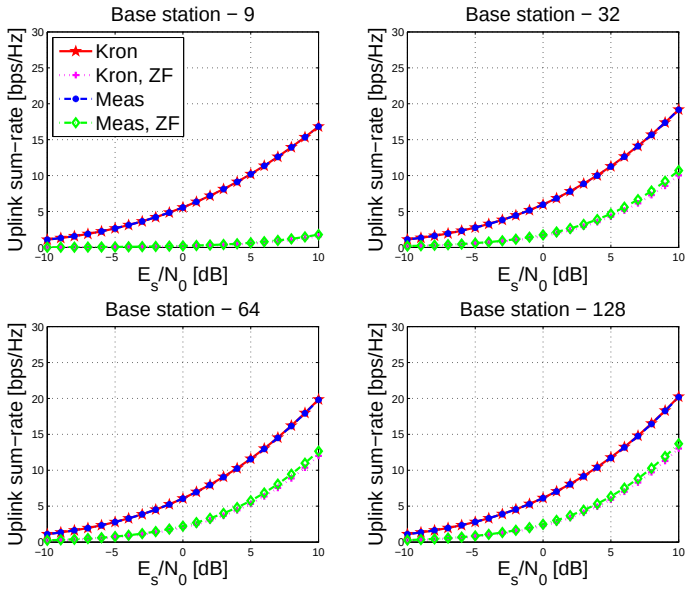

Figure 4.17: Validation of the Kronecker model. Measurement campaign: UCA with 9 synchronized users - outdoor; User location: MS 1; Propagation condition: LOS - Crowd.

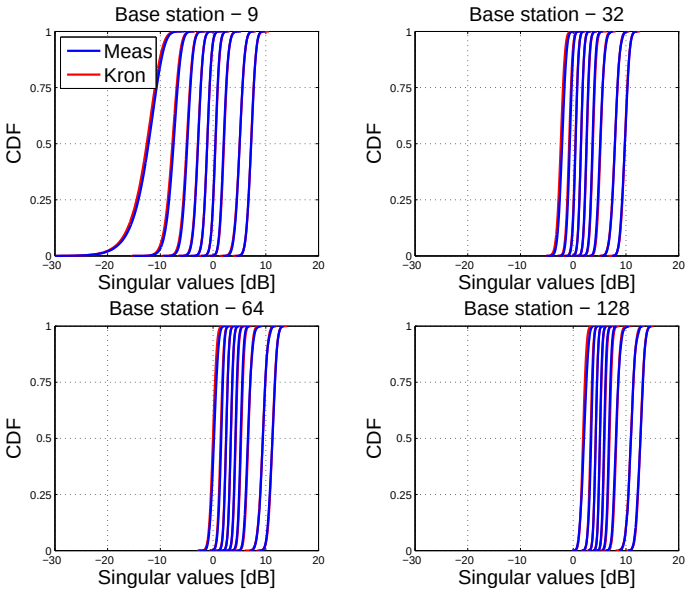

Figure 4.18: CDFs of singular values for the 9 users in measured and the Kronecker model channel. Measurement campaign: UCA with 9 synchronized users - outdoor; User location: MS 1; Propagation condition: LOS - Crowd.

To the best of our knowledge, the Kronecker model consistently underestimates the sum-rates of the channels, however, in this scenario, it has been shown to be accurate for characterizing real-life channels. Thus, it is reasonable to state that the Kronecker model does a good job of simulating the measured channel. As a matter of fact, since the number of the scatterers limits the achievable sum-rates, the uplink capacity and the ZF sum-rate for both the measure channels and the kronecker model do not increase that significantly as the number of the antenna at BS, when having more antennas (>9).

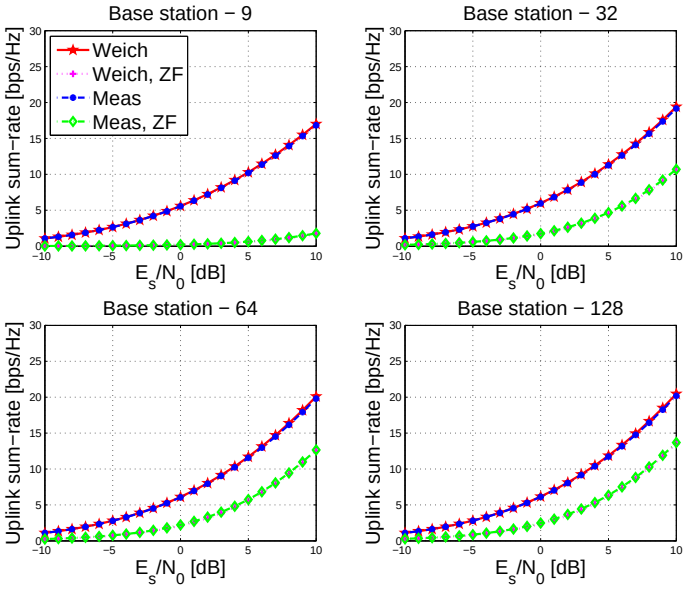

Figure 4.19: Validation of the Weichselberger model. Measurement campaign: UCA with 9 synchronized users - outdoor; User location: MS 1; Propagation condition: LOS - Crowd.

Figure 4.18 reveals that the median of singular value spreads are 19 dB, 12 dB, 11 dB and 10 dB for all the cases of 9, 32, 64 and 128 BS antennas for the measured channels, and 19.5 dB, 12 dB, 11 dB and 10 dB for the Kronecker model. Results show that the median values become smaller as increasing the number of antennas at BS. That means that user channel decorrelate if we increase the number of the antennas at BS, that can decrease the correlation between the channels and leads to a much better channel orthogonality in the measured channels and the Kronecker model.

The validation results for the Weichselberger model using the same LOS scenario are shown in the Figure 4.19. It is also noteworthy that the two

correlative models show the same performance, by seeing Figure 4.17 and Figure 4.19.

As discussed in the [15], the Kronecker model performs poorly for the larger number of antenna when using real-life data. However, the performance metrics for this scenario imply that the Kronecker model can handle the measured data obtained from a large number of antennas system. And, we, here, demonstrate once again the Weichselberger model is not more accurate than the Kronecker model.

For Weichselberger model, the median of singular value spreads are 19 dB, 11.5 dB, 10 dB and 10 dB when BS uses 9, 32, 64 and 128 antenna elements (see Figure 4.20). In such a case, it give the same performance as shown in Figure 4.18.

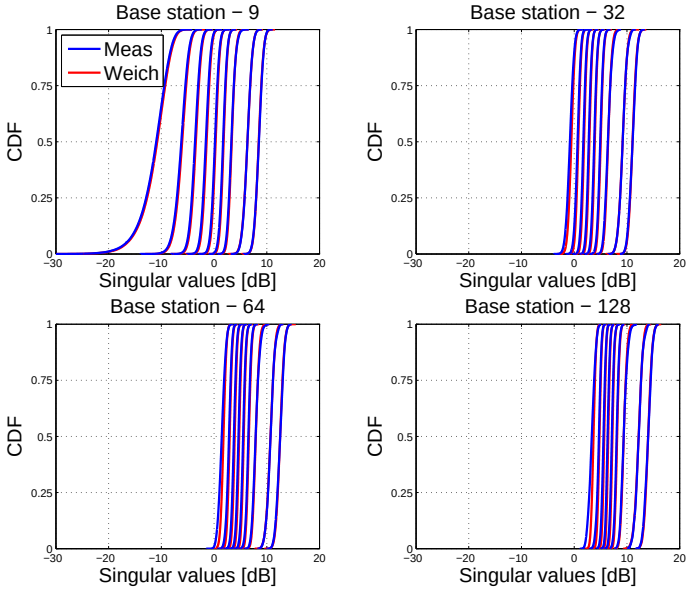

Figure 4.20: CDFs of singular values for the 9 users in measured and the Weichselberger model channel. Measurement campaign: UCA with 9 synchronized users - outdoor; User location: MS 1; Propagation condition: LOS - Crowd.

Let us next consider the case where there are no crowd in the location MS 1. In such a case, it can be more possible to point out the contribution of the crowd.

The uplink capacity and the ZF sum-rate for both the measured channels and the Kronecker model have been shown in Figure 4.21. The figure presents the same characteristics as Figure 4.17, and we can not look at the difference between them.

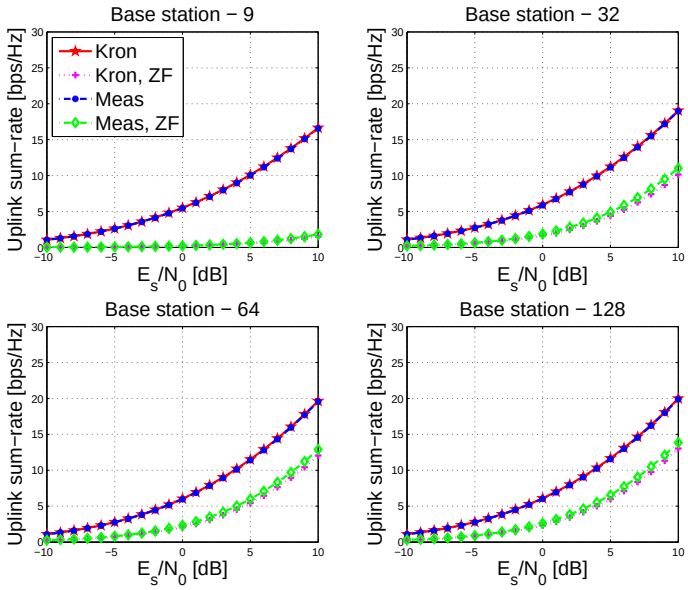

Figure 4.21: Validation of the Kronecker model. Measurement campaign: UCA with 9 synchronized users - outdoor; User location: MS 1; Propagation condition: LOS - No Crowd.

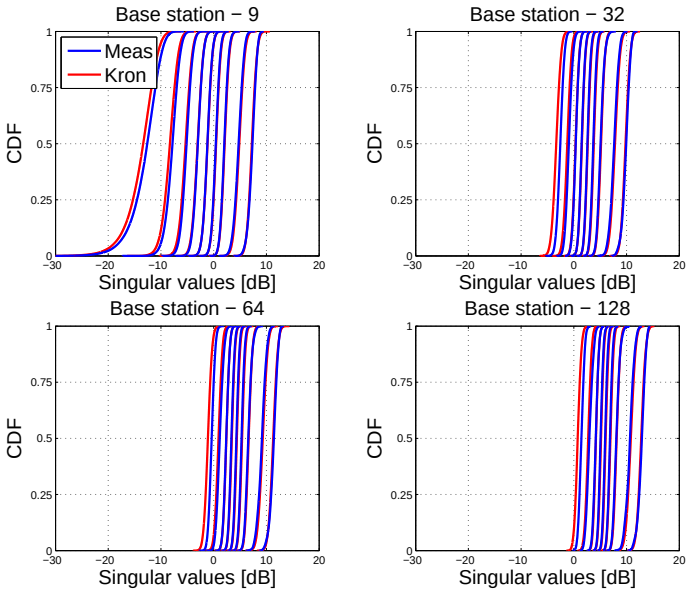

Figure 4.22: CDFs of singular values for the 9 users in measured and the Kronecker model channel. Measurement campaign: UCA with 9 synchronized users - outdoor; User location: MS 1; Propagation condition: LOS - No Crowd.

According to Figure 4.22, the median of singular value spreads for the LOS with crowd scenario are 19.5 dB, 12 dB, 11.5 dB and 11 dB for the measured channel, and are 20 dB, 13 dB, 12 dB 12 dB for the Kronecker when equipping with 9, 32, 64 and 128 antennas, respectively. This can identify with the CDFs of singular values, as shown in Figure 4.18.

By Figure 4.23, we can see that the uplink capacity and the ZF sum-rate for both the measured channels and the Weicheselberger model in the LOS condition with no crowd follow the same features of the Figure 4.19.

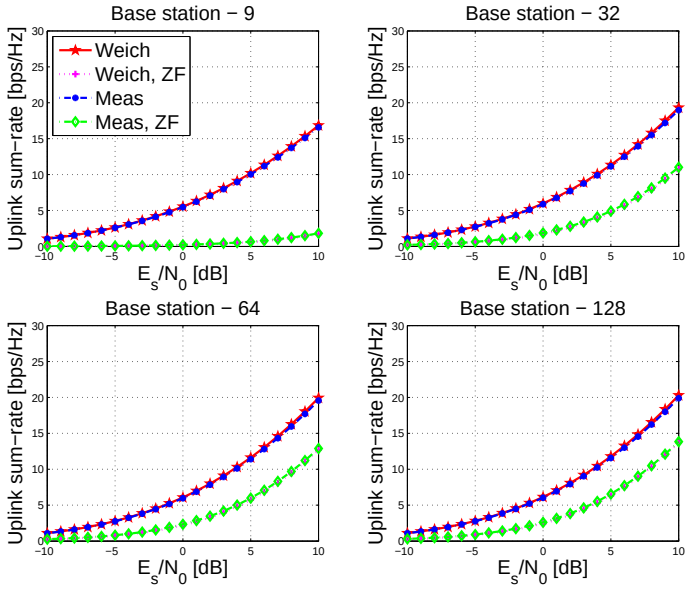

Figure 4.23: Validation of the Weichselberger model. Measurement campaign: UCA with 9 synchronized users - outdoor; User location: MS 1; Propagation condition: LOS - No Crowd.

Figure 4.24 investigates the behaviour of the CDFs of singular values for the Weichselberger model based on the LOS condition without crowd environment. The simulated curves not only present that the median of singular value spreads for the Weichselberger model are 19 dB, 12 dB, 11 dB and 11 dB (M = 9, 32, 64 and 128), but also depict that it is a trustworthy model for the measured data.

To the end, our general comments are that when we consider this LOS scenario in the future, the Kronecker model and the Weichselberger model can play a great role in simulating this kind of environment. However, the designed crowd leads to a neglect-able influence for our environment, thus, it is required to define a better crowd for our environment if we want to examine the effect of the crowd.

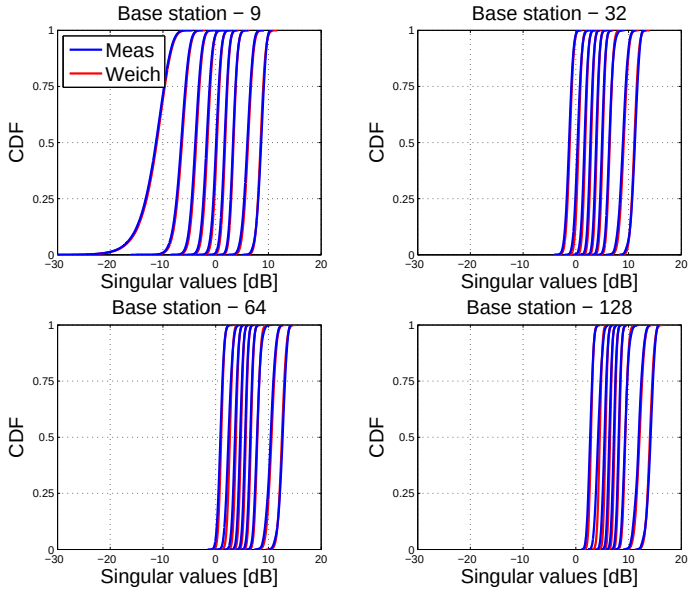

Figure 4.24: CDFs of singular values for the 9 users in measured and the Weichselberger model channel. Measurement campaign: UCA with 9 synchronized users - outdoor; User location: MS 1; Propagation condition: LOS - No Crowd.

NLOS Scenarios

For the LOS scenarios above, it reflects the simulate ability of the correlative models considered at massive MIMO channels. We now give the validation results based on the NLOS scenario in order to gain more insights for the correlative models.

As illustrate in Figure 4.25, the uplink capacity and the ZF sum-rate for both the measured channel and the Kronecker model go to a higher level compared with the LOS scenario with crowd, as shown in Figure 4.17, that is because NLOS with rich scattering allows better spatial separation of the user signals.

As the number of antenna elements at BS increases, the gap between the measured channel and the Kronecker model for the uplink capacity and the ZF sum-rate becomes smaller, since ZF pre-coding is used to remove inter symbol interference (ISI) and this process consumes some power, however, the consumption decreases when increasing the number of antenna.

Figure 4.26 shows the result of the CDFs of singular values, and according to the figure, the median of singular value spreads can be given. They are 14 dB, 6 dB, 5 dB and 4 dB as the number of the antenna elements at BS increases for the measured model, and 14.5 dB 6 dB, 5.5 dB and 5 dB

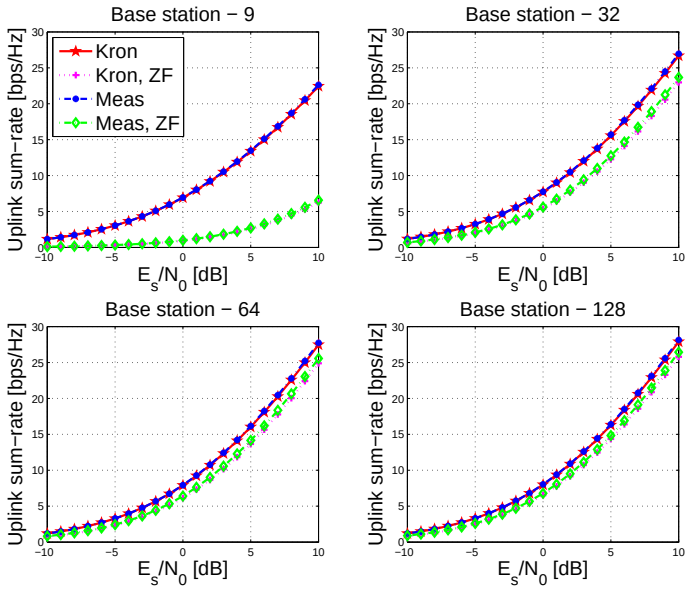

Figure 4.25: Validation of the Kronecker model. Measurement campaign: UCA with 9 synchronized users - outdoor; User location: MS 3; Propagation condition: NLOS - Crowd.

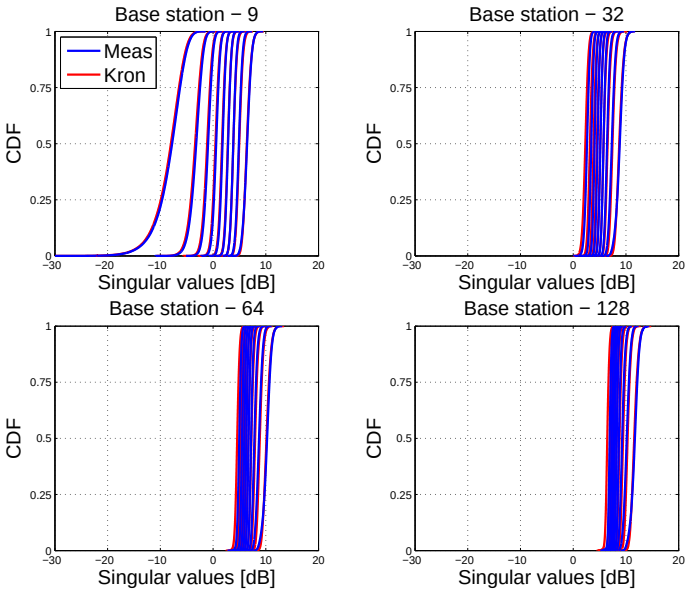

Figure 4.26: CDFs of singular values for the 9 users in measured and the Kronecker model channel. Measurement campaign: UCA with 9 synchronized users - outdoor; User location: MS 3; Propagation condition: NLOS - Crowd.

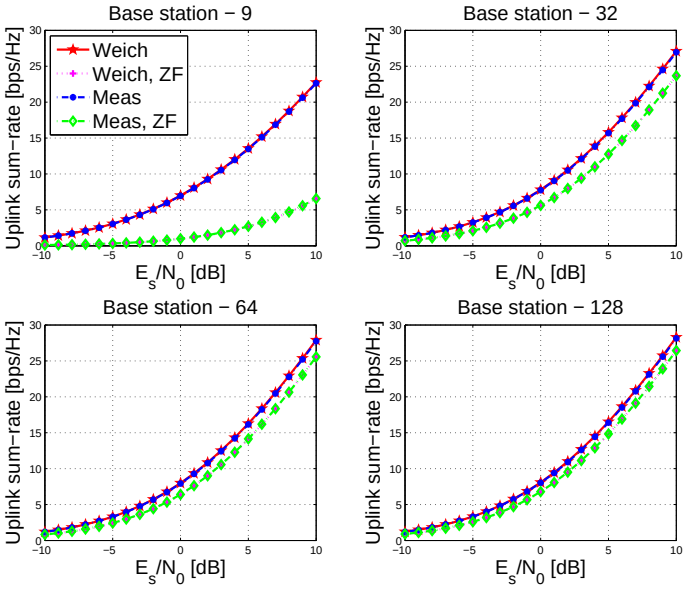

Figure 4.27: Validation of the Weichselberger model. Measurement campaign: UCA with 9 synchronized users - outdoor; User location: MS 3; Propagation condition: NLOS - Crowd.

for the Kronecker model.

It should be noted that the median values become significantly smaller in NLOS condition, as compared to those in the corresponding LOS condition. Moreover, the singular value spreads have lesser variations for the measured channel and the Kronecker model if M = 9, after that, the singular value spreads can be treated as a constant for M = 32, 64 and 128. This model provides performance very close to the measured channel and gives better spatial separation of the user signals.

It is assumed that the Weichselberger model is confirmed. By using that, the uplink capacity and the ZF sum-rate can be achieved, as illustrated in 4.27. By taking into account the figure, it is hard to be further distinguished for the measured channels and the Weichselberger model and it is also difficulty to specify the difference between this figure and the Figure 4.25. Accordingly, the two described correlative models is supposed to have ability to model the measured channel when we choose this scenario.

In Figure 4.28, the median of singular value spreads (14 dB, 6 dB 5 dB and 4.5 dB) for the Weichselberger model can be achieved according to equipping 9, 32, 64 and 128 antenna elements at BS. This figure can be explained as the Figure 4.26, as they match each other very well.

As can be seen in Figure 4.29 and Figure 4.25, both figures are the

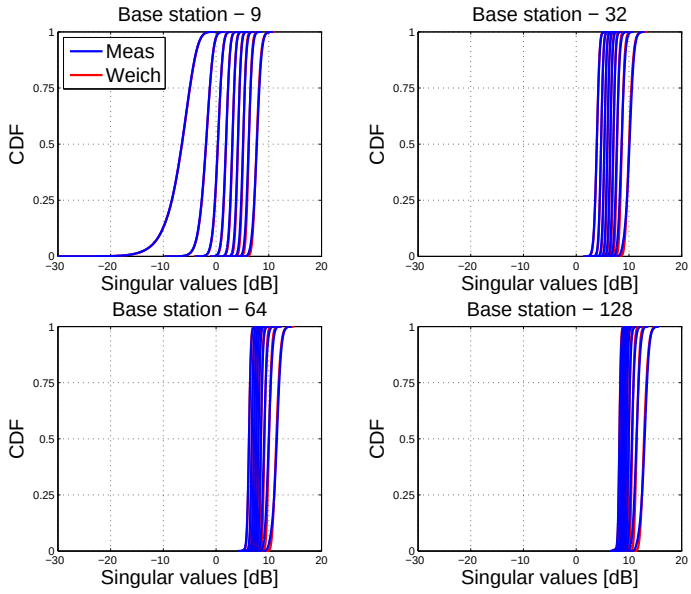

Figure 4.28: CDFs of singular values for the 9 users in measured and the Weichselberger model channel. Measurement campaign: UCA with 9 synchronized users - outdoor; User location: MS 3; Propagation condition: NLOS - Crowd.

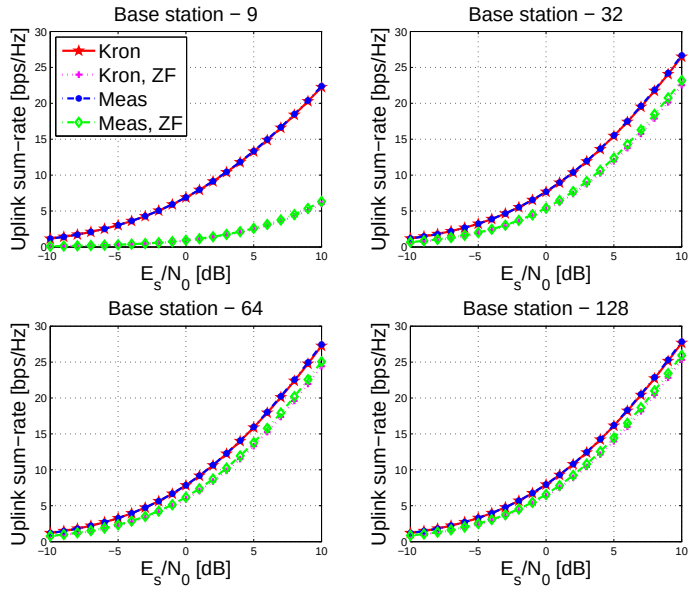

Figure 4.29: Validation of the Kronecker model. Measurement campaign: UCA with 9 synchronized users - outdoor; User location: MS 3; Propagation condition: NLOS - No Crowd.

same. Figure 4.30 and Figure 4.26 display the same characteristics. The reason for this is from the crowd, furthermore, the crowd can be ignored due to its inefficiency.

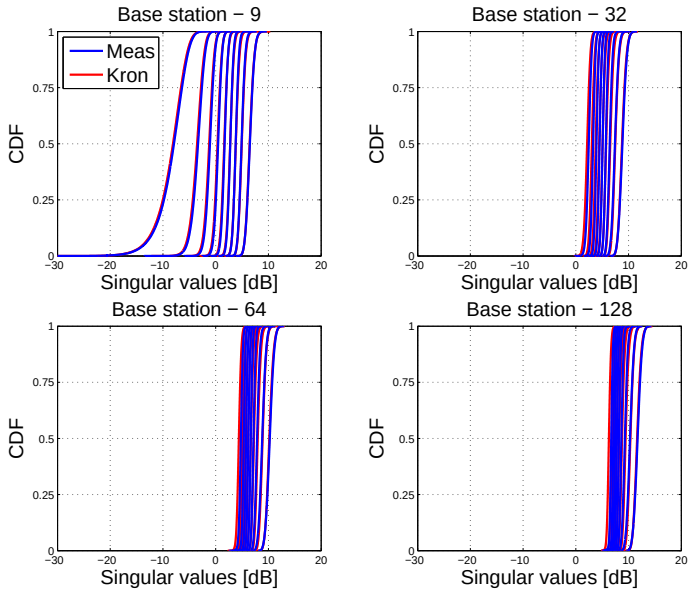

Figure 4.30: CDFs of singular values for the 9 users in measured and the Kronecker model channel. Measurement campaign: UCA with 9 synchronized users - outdoor; User location: MS 3; Propagation condition: NLOS - No Crowd.

For the Weichselberger model, it also can be shown that the crowd is hard to influence our measurement, when we comparing the Figure 4.31 and 4.27 as well as the Figure 4.32 and the Figure 4.28.

Reviewing the simulation results for the third measurement campaign, we must point out three key statements. Firstly, the Kronecker model and the Weichselberger model do a good job of representing the measured data obtained in this measurement campaign, as the singular values of the model channel predicted by the correlative models closely follow those of the measured channel. Secondly, despite the Weichselberger model has been provided to be more accurate than the Kronecker model, the two models make an equal contribution for our data. Finally, unfortunately, the crowd is of no effect when adding it to our measurement. Thus, in the future, a new method is needed to set the crowd.

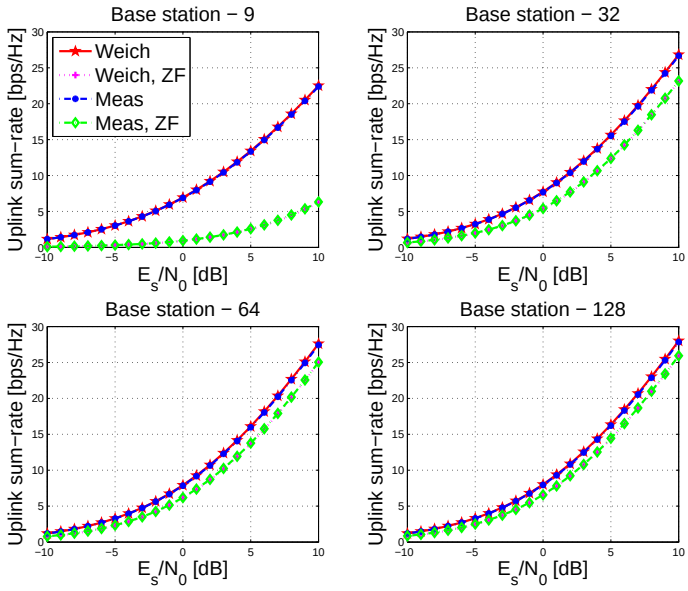

Figure 4.31: Validation of the Weichselberger model. Measurement campaign: UCA with 9 synchronized users - outdoor; User location: MS 3; Propagation condition: NLOS - No Crowd.

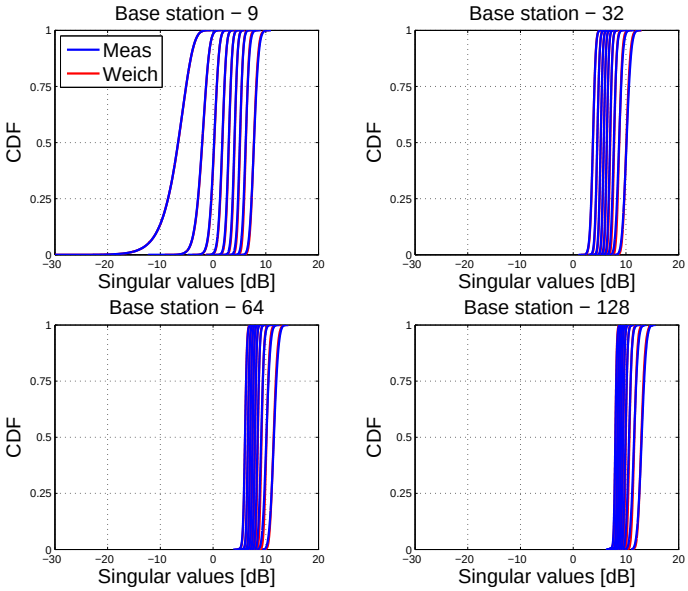

Figure 4.32: CDFs of singular values for the 9 users in measured and the Weichselberger model channel. Measurement campaign: UCA with 9 synchronized users - outdoor; User location: MS 3; Propagation condition: NLOS - No Crowd.

4.2.4 UCA with 9 Synchronized Users - Indoor

Expect for the concluded three measurement campaign, the simulation results for the last measurement campaign presented in this section hold for the indoor environment. It is clear that all scenarios own LOS conditions by viewing the Figure 2.4.

To facilitate our analysis, we here show the results of the scenarios according to the positions of the BS, as following:

- Firstly, the scenario employs the BS 1, as shown in Figure 2.4a. The users with and without the crowd displayed in Figure 2.4b stay at the 20 seats of the Group 1.
- The second scenario is based on the first scenario, but follows the BS 3 instead of BS 1.

BS Location 1

We take Figure 4.33 as a starter to show the validation results of the Kronecker model. It is easy to see that the gap between the measured channels and the Kronecker model becomes lesser, as the number of antennas at BS increases, for the uplink capacity and the ZF sum-rate.

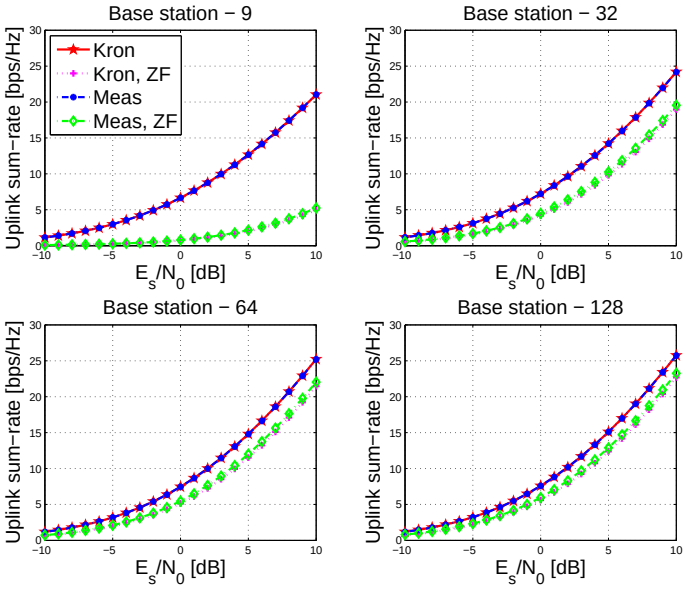

Figure 4.33: Validation of the Kronecker model. Measurement campaign: UCA with 9 synchronized users - indoor; BS location: BS 1; Crowd: Yes.

By comparing to the outdoor scenario, we observe that the uplink capacity and the ZF sum-rate go to a higher level and the gap between become smaller, for 9, 32, 64 and 128 antennas, respectively (see Figure 4.17).

Figure 4.34 shows the CDFs of singular values when using BS 1 with crowd. From the figure, the median of singular value spreads can be found, that are 16 dB, 9 dB, 8 dB and 7 dB for the measured channel when equipping with 9, 32 64 and 128 antenna elements at BS, further, 16 dB, 9 dB, 8 dB and 7 dB for the Kronecker model. We note that the medians are equal for the measured and the model, that indicates that in this scenario, the Kronecker model is a perfect model to follow the measured channel. Furthermore, it is still shows a good performance, as compared to outdoor scenario (see Figure 4.18).

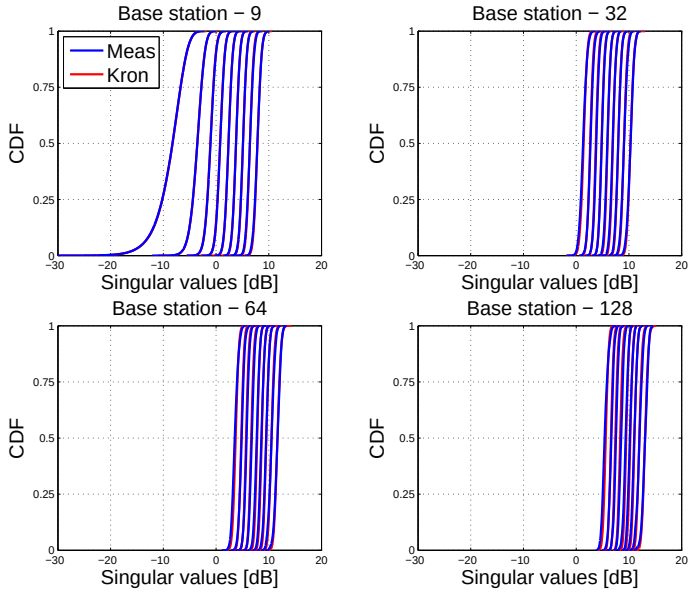

Figure 4.34: CDFs of singular values for the 9 users in measured and the Kronecker model channel. Measurement campaign: UCA with 9 synchronized users - indoor; BS location: BS 1; Crowd: Yes

Here, we present the uplink capacity and ZF sum-rate for both the measured channel and the Weichselberger model in Figure 4.35. By recalling the same validation metrics in the outdoor with LOS condition (see Figure 4.19), it is easy to know that the validation metrics achieved in the indoor environment are higher than those achieved in the outdoor environment. On the other hand, the ZF sum-rate is close to the uplink capacity for both the measured channel and the Weichselberger model, when the number of the antenna elements at BS increases.

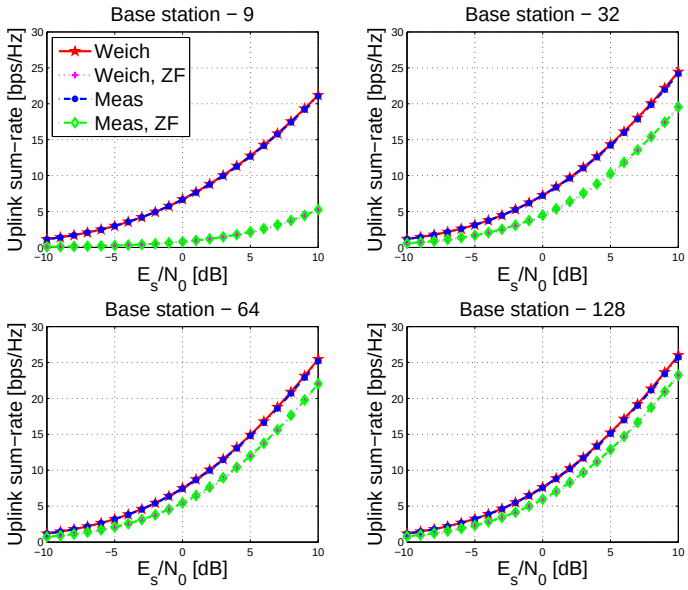

Figure 4.35: Validation of the Weichselberger model. Measurement campaign: UCA with 9 synchronized users - indoor; BS location: BS 1; Crowd: Yes.

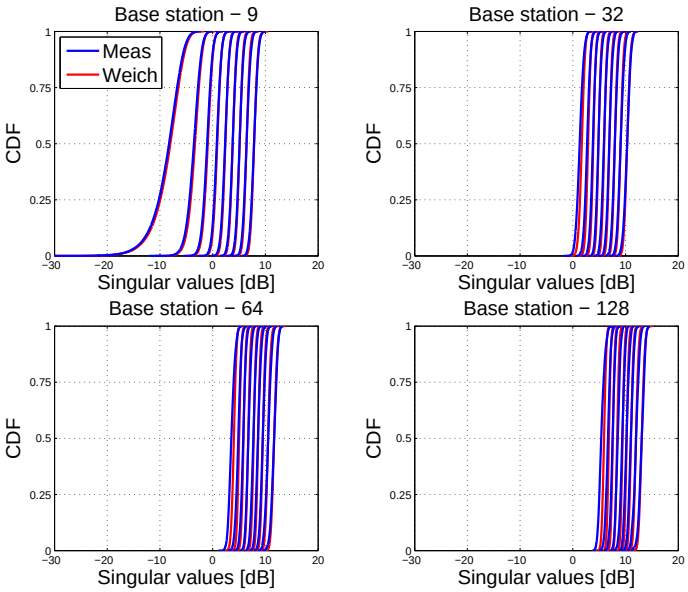

Figure 4.36: CDFs of singular values for the 9 users in measured and the Weichselberger model channel. Measurement campaign: UCA with 9 synchronized users - indoor; BS location: BS 1; Crowd: Yes

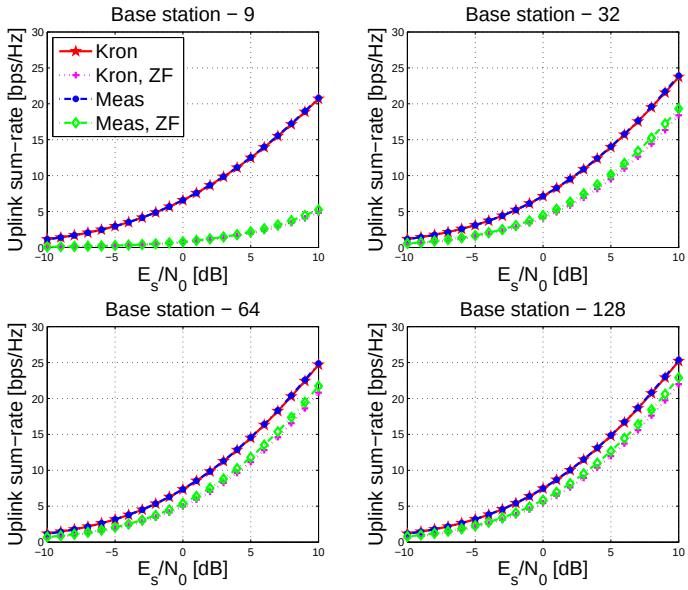

Figure 4.37: Validation of the Kronecker model. Measurement campaign: UCA with 9 synchronized users - indoor; BS location: BS 1; Crowd: No.

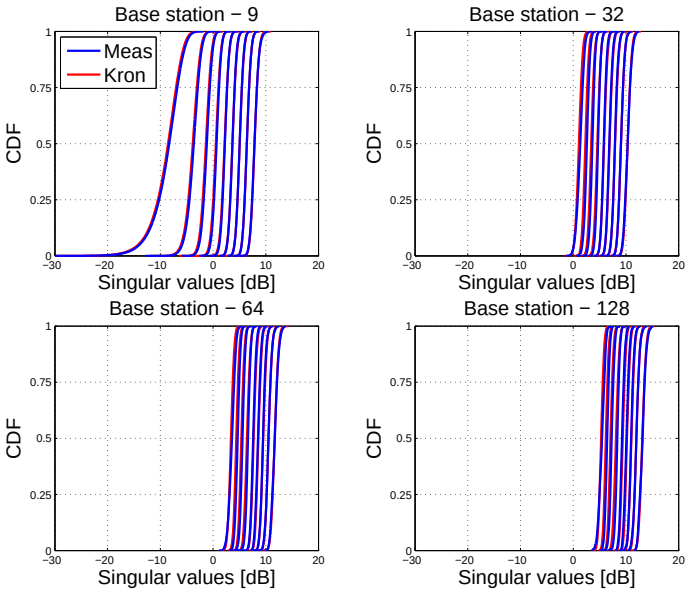

Figure 4.38: CDFs of singular values for the 9 users in measured and the Kronecker model channel. Measurement campaign: UCA with 9 synchronized users - indoor; BS location: BS 1; Crowd: No.

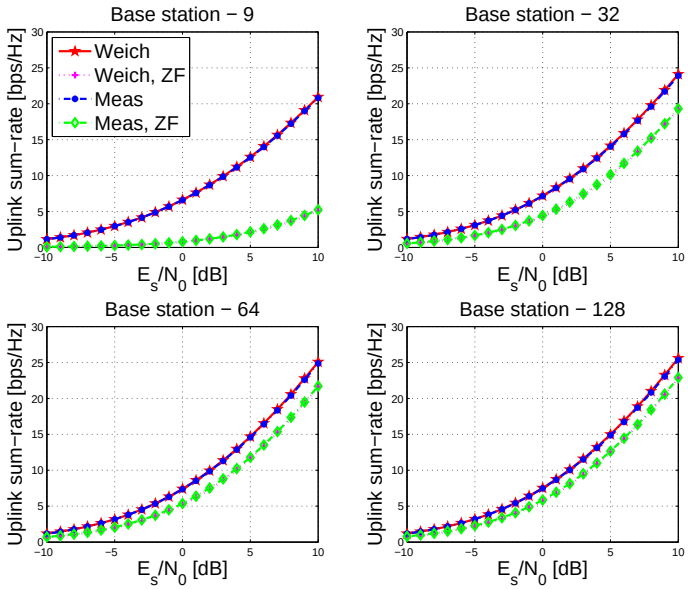

Figure 4.39: Validation of the Weichselberger model. Measurement campaign: UCA with 9 synchronized users - indoor; BS location: BS 1; Crowd: No.

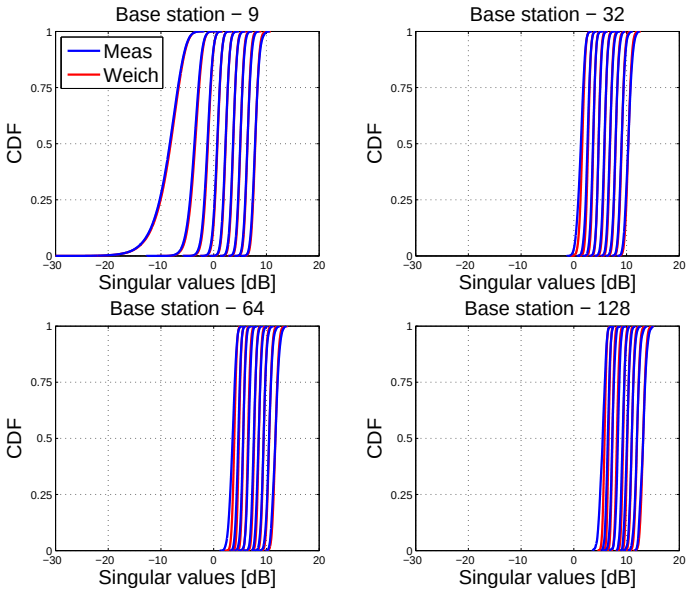

Figure 4.40: CDFs of singular values for the 9 users in measured and the Weichselberger model channel. Measurement campaign: UCA with 9 synchronized users - indoor; BS location: BS 1; Crowd: No.

Figure 4.36 gives the CDFs of singular values for the measured channel and the Weichselberger model, when using BS 1 with the crowd. We can observe that the median of singular value spreads are 16 dB, 8 dB, 7.5 dB and 7 dB, for M = 9, 32, 64 and 128. After that, it can be seen that the match between the model and the measured channel is well and the the tails of the CDF curves disappear when using more than 9 antennas at BS.

As shown in Figure 4.37 and Figure 4.38, the simulation results are got when using BS 1 with crowd. As already known, the crowd for our measurement has no impact on the system performance. Unfortunately, it is clear to give that for this scenario, the crowd also makes a little contribution to the system performance when compared with Figure 4.33 and Figure 4.34.

Because of the null crowd, the validation results for the Weichselberger model (Figure 4.39 and Figure 4.40) can lead to the same characteristics as Figure 4.35 and Figure 4.36.

BS Location 3

To gain more insights, we do the simulation according to the indoor environment by changing the BS 1 into BS 3. It is worth point out that the uplink capacity and the ZF sum-rate for both the measured channel and the

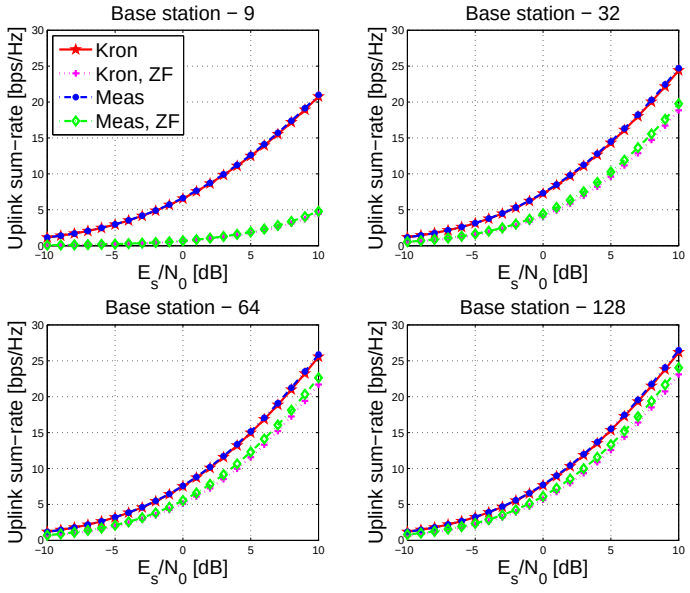

Figure 4.41: Validation of the Kronecker model. Measurement campaign: UCA with 9 synchronized users - indoor; BS location: BS 3; Crowd: Yes.

Kronecker model (see Figure 4.41) can be found the same as Figure 4.33. That is noted that in indoor scenario, the improving of the performance goes to zero when changing the distance between the users and the BS.

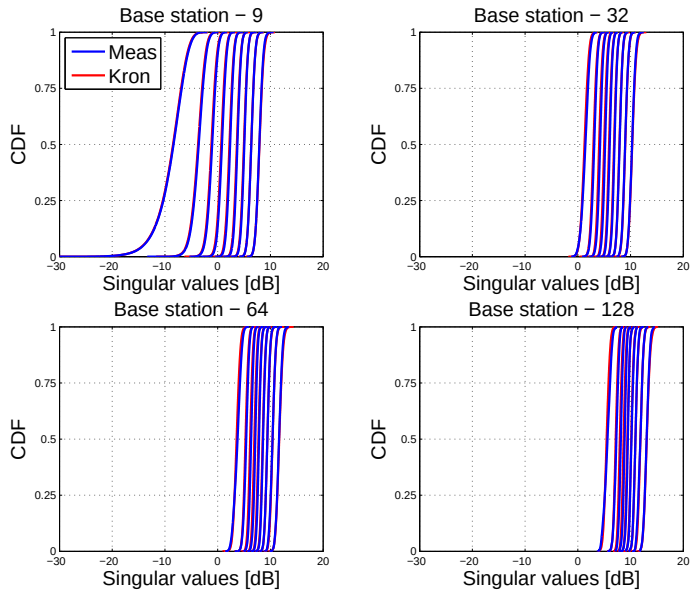

Figure 4.42: CDFs of singular values for the 9 users in measured and the Kronecker model channel. Measurement campaign: UCA with 9 synchronized users - indoor; BS location: BS 3; Crowd: Yes.

From the CDFs of singular values in Figure 4.42, the median of singular value spreads are 16 dB, 8.5 dB, 7.5 dB and 7 dB for the measured channel, 16 dB, 9 dB, 8 dB and 7 dB for the Kronecker model when equipping 9, 32, 64 and 128 antenna elements at BS. The match for the measured channel and the Kronecker model is worse than those shown in Figure 4.34, that is because the BS 1 is closer to Group 1 than the BS 3 as shown in Figure 2.4a.

Comparing Figure 4.43 with Figure 4.35, we can see that the twin figures are obvious. Thus, in this case, BS 1 and BS 3 can support the same unlink capacity and ZF sum-rate for the measured channel and the Weichselberger model.

From Figure 4.44, the median of singular value spreads are 16 dB, 8.5 dB, 7.5 dB and 7 dB for all the cases of 9, 32, 64 and 128 antenna elements, respectively. For the comparison with Figure 4.36, this figure also gives worse match since the BS 3 is farther to users than the BS 1.

In the following, the validation results are achieved by employing the BS 3 without the crowd. Since the validation results for the Kronecker model (Figure 4.45 and Figure 4.46) are considered as the same with those

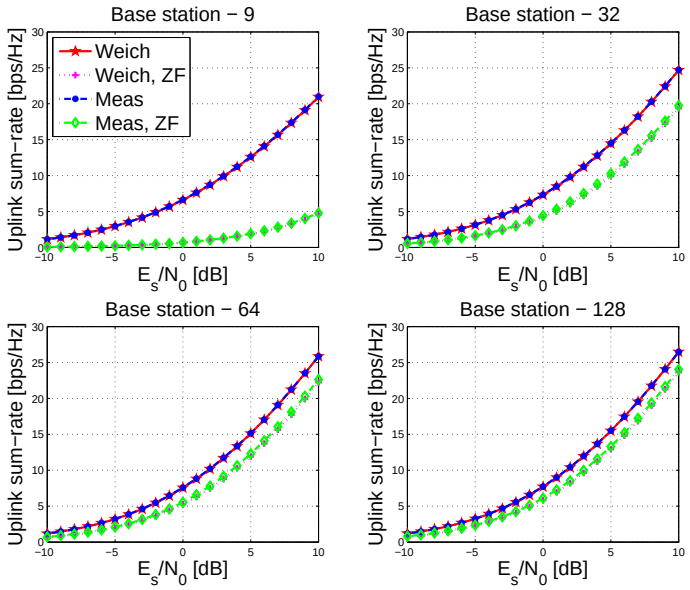

Figure 4.43: Validation of the Weichselberger model. Measurement campaign: UCA with 9 synchronized users - indoor; BS location: BS 3; Crowd: Yes.

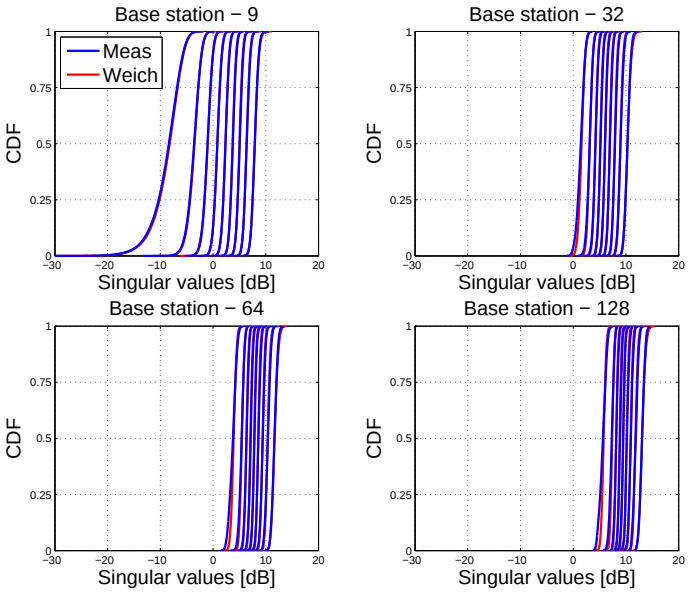

Figure 4.44: CDFs of singular values for the 9 users in measured and the Weichselberger model channel. Measurement campaign: UCA with 9 synchronized users - indoor; BS location: BS 3; Crowd: Yes.

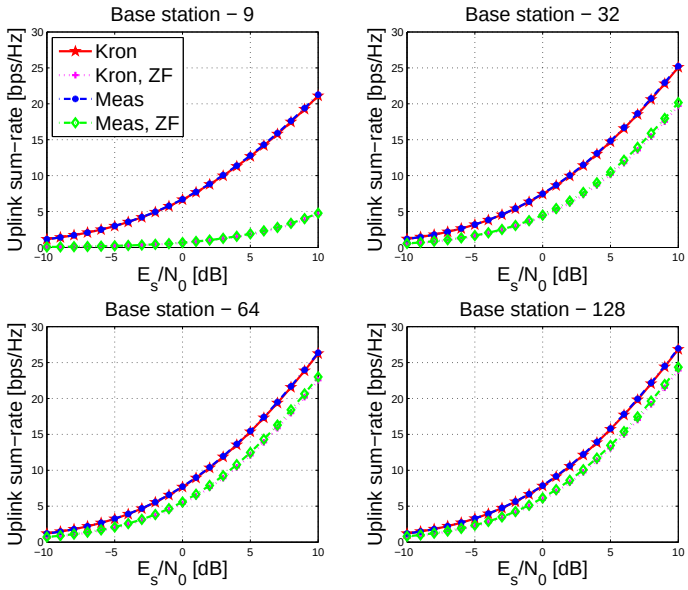

Figure 4.45: Validation of the Kronecker model. Measurement campaign: UCA with 9 synchronized users - indoor; BS location: BS 3; Crowd: No.

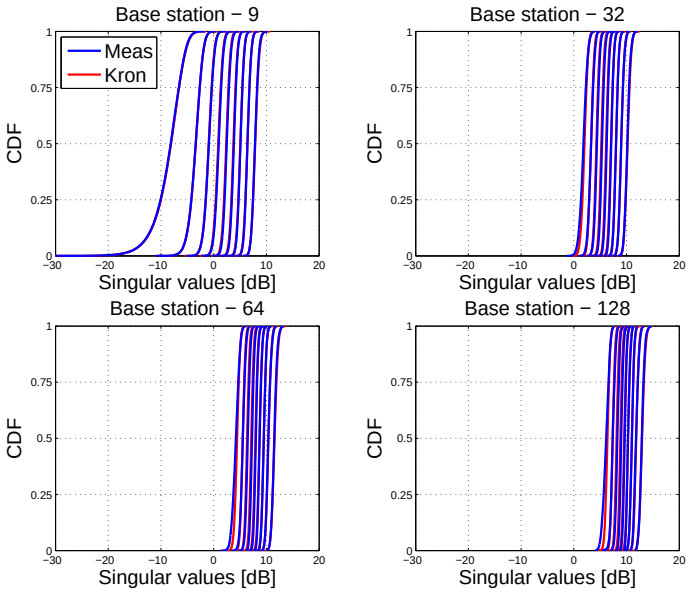

Figure 4.46: CDFs of singular values for the 9 users in measured and the Kronecker model channel. Measurement campaign: UCA with 9 synchronized users - indoor; BS location: BS 3; Crowd: No.

obtained in crowd (Figure 4.41 and Figure 4.42) and the validation results for the Weichselberger model (see Figure 4.47 and Figure 4.48) also achieve the same validation results, as shown in Figure 4.43 and Figure 4.44, we do not give more comments for them.

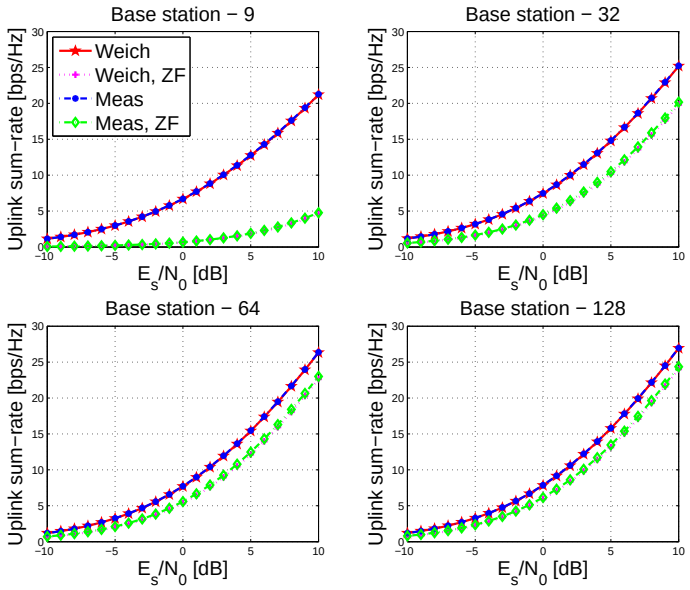

Figure 4.47: Validation of the Weichselberger model. Measurement campaign: UCA with 9 synchronized users - indoor; BS location: BS 3; Crowd: No.

In this chapter, we present an experimental analysis of the correlative channel models by choosing typical scenarios, and validation results of all scenarios will be given in the Chapter 5. To the end, two comments to the development of massive MIMO for this chapter can be summarized as follows:

1. As already known, the crowd has no impact on the system performance and it is required to seek a good method to set the crowd if we want to investigate the influence of the crowd in the future.

2. Cylindrical array supports higher advantages than linear array.

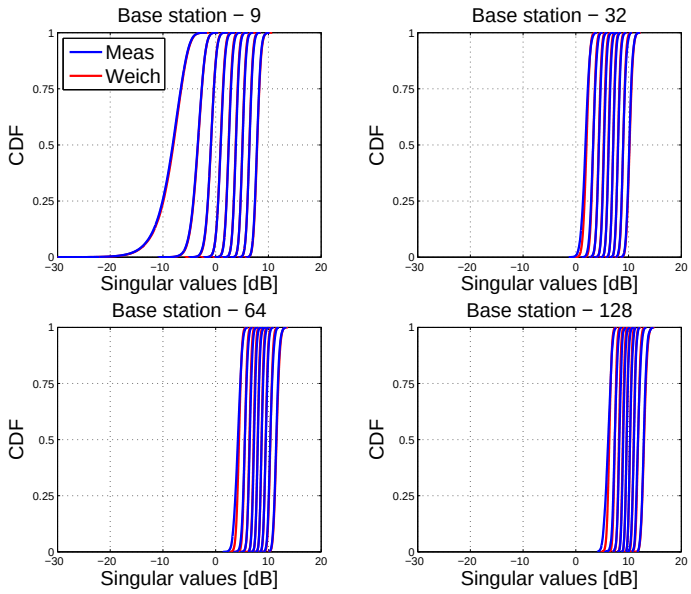

Figure 4.48: CDFs of singular values for the 9 users in measured and the Weichselberger model channel. Measurement campaign: UCA with 9 synchronized users - indoor; BS location: BS 3; Crowd: No.

Chapter 5

Summary Results of the Correlative Models

We have validated the two correlative models by using real-life data from some typical scenarios in the Chapter 4. Also, real-life data given by all scenarios from each measurement campaign have been used to develop the two correlative models. After that, two validation metrics the uplink capacity and the ZF sum-rate were computed according to the generated correlative models.

When considering one measurement campaign, both the uplink capacity and the ZF sum-rate for each scenario are extracted at $E_s/N_0 = 10$ dB. And in order to evaluate the correlative models, we summarize all the extracted ZF sum-rates for each measurement campaign as well as the extracted uplink capacities in this chapter.

5.1 Linear Array

5.1.1 ULA with 5 Virtual Users

Figure 5.1 shows the modelled versus measured uplink capacity for the Kronecker model and the Weichselberger model , when having 5, 32, 64 and 128 antennas at BS. The diagonal represents the case of no model error. For each model, a specific marker corresponds to one scenario, and there are 9 scenarios in the first measurement campaign. The kronecker model (red squares) and the Weichselberger model (blue circles) underestimate the measured uplink capacity. The reason for this is due to the larger aperture of the ULA. Moreover, the mismatch goes to 50% for the Kronecker model and 20% for the Weichselberger model. Since the Weichselberger model considers the coupling coefficients between the transmit side and the receive side, it has a lower mismatch than the Kronecker model.

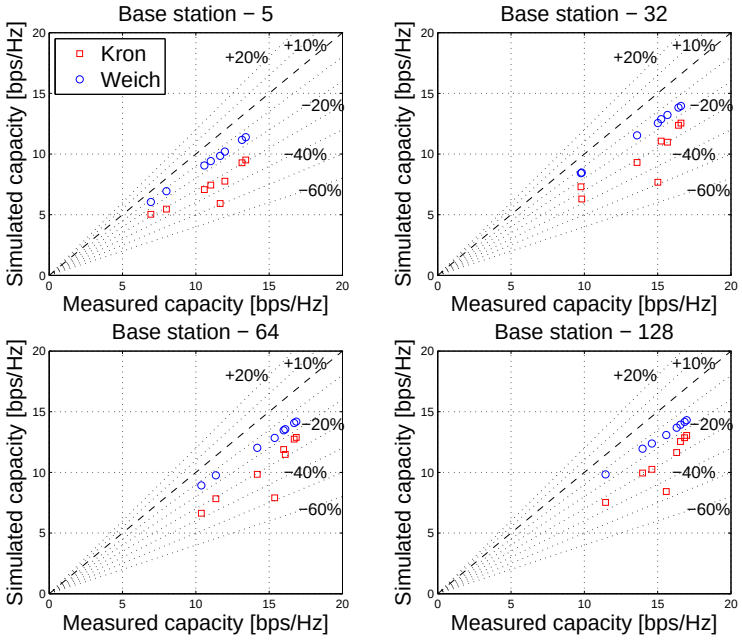

Figure 5.1: The uplink capacity of Measured versus Modeled for the measurement campaign "ULA with 5 virtual users" at a E_s/N_0 of 10 dB.

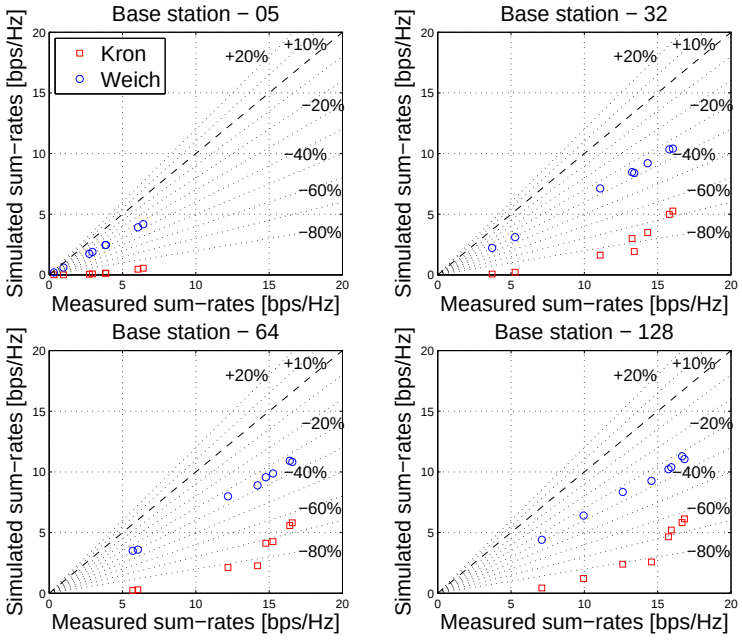

Figure 5.2: The Zero-forcing sum-rates of Measured versus Modeled for the measurement campaign "ULA with 5 virtual users" at a E_s/N_0 of 10 dB.

Figure 5.2 shows a modelled versus measured ZF sum-rate graph for all scenarios from the first measurement campaign. The two correlative models underestimate significantly the measured ZF sum-rate. And it is obvious to show that the improvement of the ZF sum-rate for the two correlative models when the number of the antenna elements is larger (>5). That is because ZF pre-coder consumes less power as increasing the number of antennas at BS, which results in the ZF sum-rate become larger and close to the measured ZF sum-rate.

5.2 Cylindrical Array

5.2.1 UCA with 5 Virtual Users

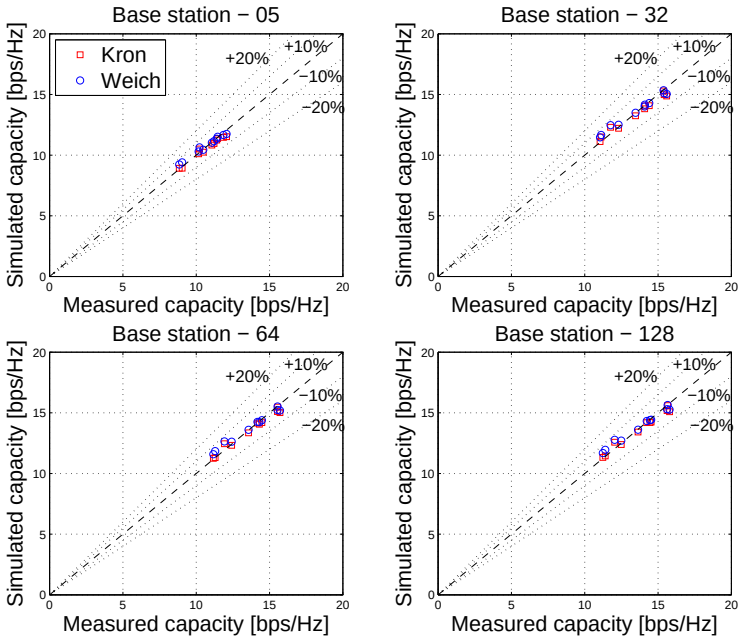

Figure 5.3: The uplink capacity of Measured versus Modeled for the measurement campaign "UCA with 5 virtual users" at a E_s/N_0 of 10 dB.

It is observed from the Figure 5.3 that the UCA gives higher advantages than the ULA when comparing with Figure 5.1. All scenarios are from the second measurement campaign and the uplink capacity for each scenario are summarized in Figure 5.3. In general, the Kronecker model and the Weichselberger model fit the measurements best with relative errors within a few percents for the all cases of 5, 32, 64 and 128 antennas.

As with the scenarios from the second measurement campaign, the ZF sum-rates for all scenarios are shown in Figure 5.3. When considering 5 antennas at BS, the Kronecker model error is 20% for all scenarios, whereas that of the Weichselberger model is 5%. However, when having more than 5 antennas, the ZF sum-rate for both models improve significantly and the two correlative models error remains relatively constant regardless of array size.

For the second measurement campaign, note that for all scenarios, both the uplink capacity and the ZF sum-rate extend to a longer interval, as having more antennas at BS (>5). As mentioned in Chapter 4, the environment for this measurement campaign fluctuates rapidly, that leads to the extension for the uplink capacity and the ZF sum-rate.

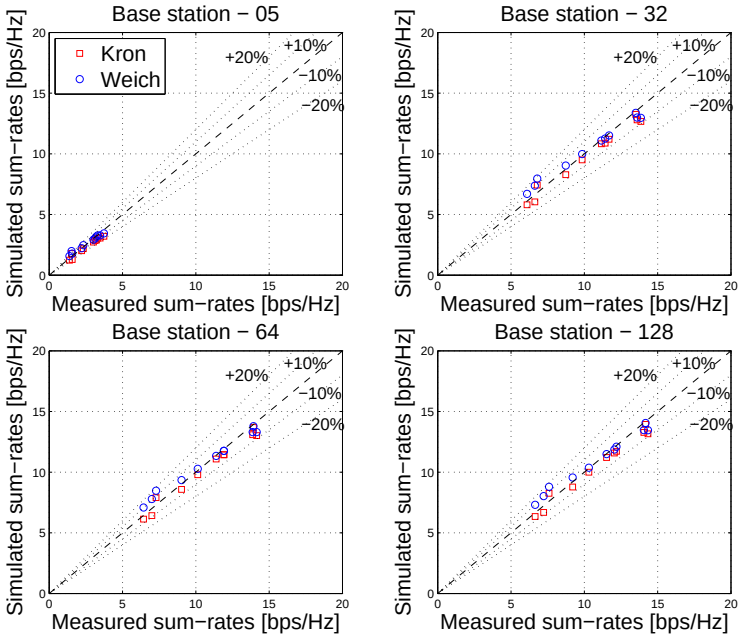

Figure 5.4: The Zero-forcing sum-rates of Measured versus Modeled for the measurement campaign "UCA with 5 virtual users" at a E_s/N_0 of 10 dB.

5.2.2 UCA with 9 Synchronized Users - Outdoor

In Figure 5.5, the modelled versus measured uplink capacity for all scenarios listed in the third measurement campaign is shown. The Kronecker model and the Weichselberger model perform quite well overall for equipping 9, 32, 64 and 128 antennas at BS. The two correlative models error for all scenarios shows almost zero and remains zero regardless of array size.

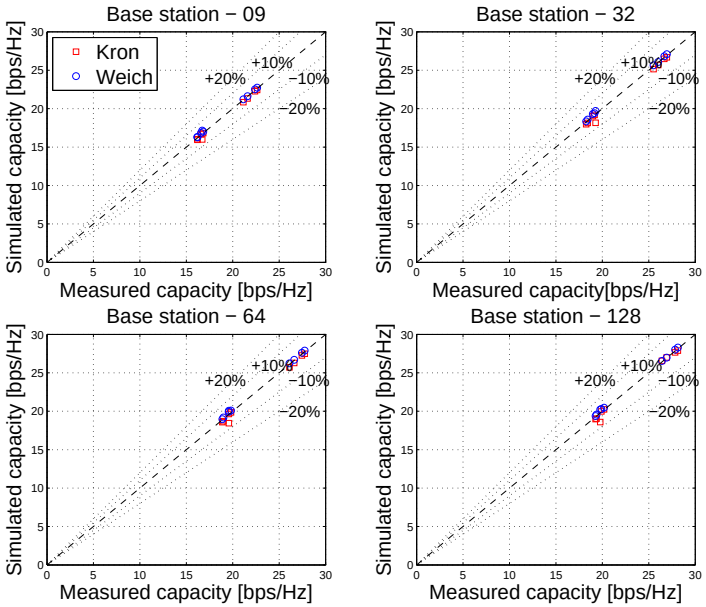

Figure 5.5: The uplink capacity of Measured versus Modeled for the measurement campaign "UCA with 9 synchronized users - outdoor" at a E_s/N_0 of 10 dB.

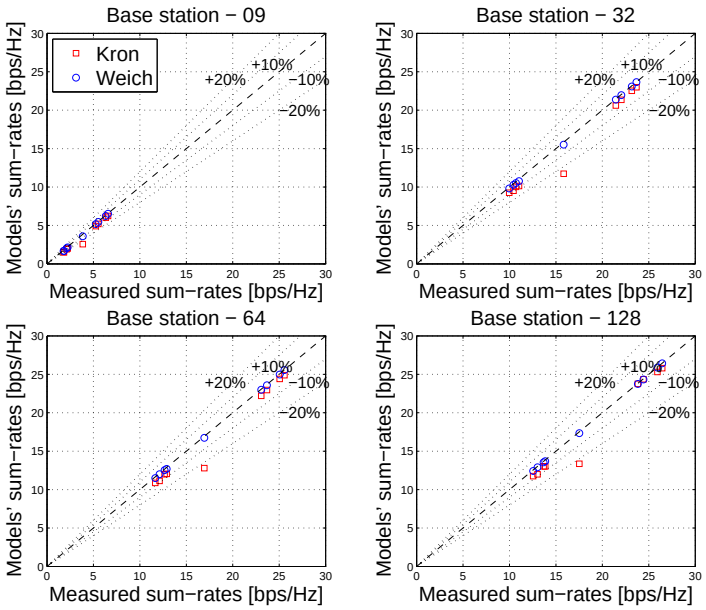

Figure 5.6: The Zero-forcing sum-rates of Measured versus Modeled for the measurement campaign "UCA with 9 synchronized users - outdoor" at a E_s/N_0 of 10 dB.

On the other hand, it is also pointed that some markers with higher uplink capacity are from the scenarios with NLOS condition and the rest markers with lower uplink capacity are built in the scenarios with LOS condition, this is because the NLOS conditions given rich scattering can allow a much better spatial separation of user signals.

Figure 5.6 illustrates the modelled versus measured ZF sum-rate for all scenarios achieved in the third measurement campaign. It shows the Weichselberger model (blue circles) performs best for all antenna deployments. For the Kronecker model, it underestimates the measured ZF sum-rate for equipping 9, 32, 64 and 128 antennas. Furthermore, from the NLOS scenarios to the LOS scenarios, the mismatch for the Kronecker model increases for all cases.

The special points can be found in Figure 5.6 that obviously underestimated the measured channel is a different case that have not been discussed before. The users are well-separated at four measurement sites in measurement campaign "UCA with 9 synchronized users - outdoor".

5.2.3 UCA with 9 Synchronized Users - Indoor

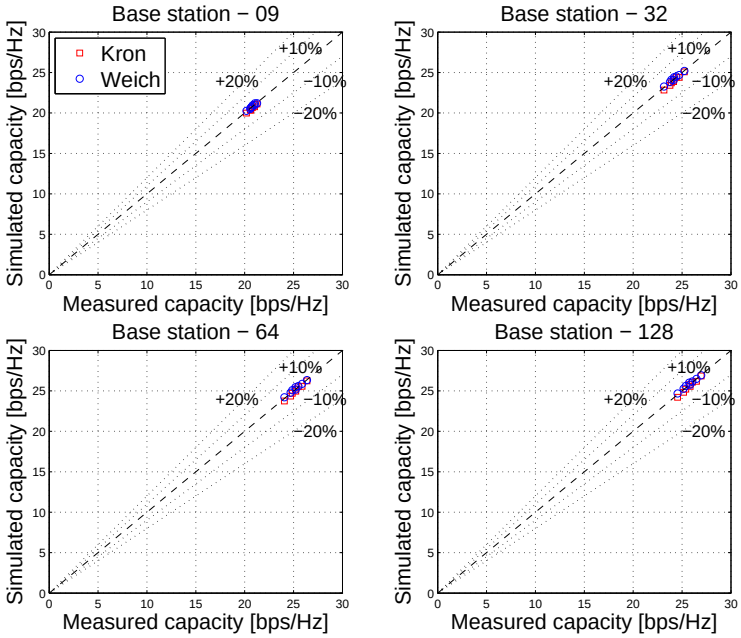

Figure 5.7: The uplink capacity of Measured versus Modeled for the measurement campaign "UCA with 9 synchronized users - indoor" at a E_s/N_0 of 10 dB.

Let us investigate the two correlative models according to indoor scenarios from the last measurement campaign, as shown in Figure 5.7. For all scenarios, both the uplink capacity and the ZF sum-rate always stay on the diagonal regardless of array size. That means that both the Kronecker model and the Weichselberger model have no model error and perfect match. On the other hand, since LOS component serves for every scenario, the uplink capacity and the ZF sum-rate for both models have a relative smaller fluctuation, when considering all antenna deployments.

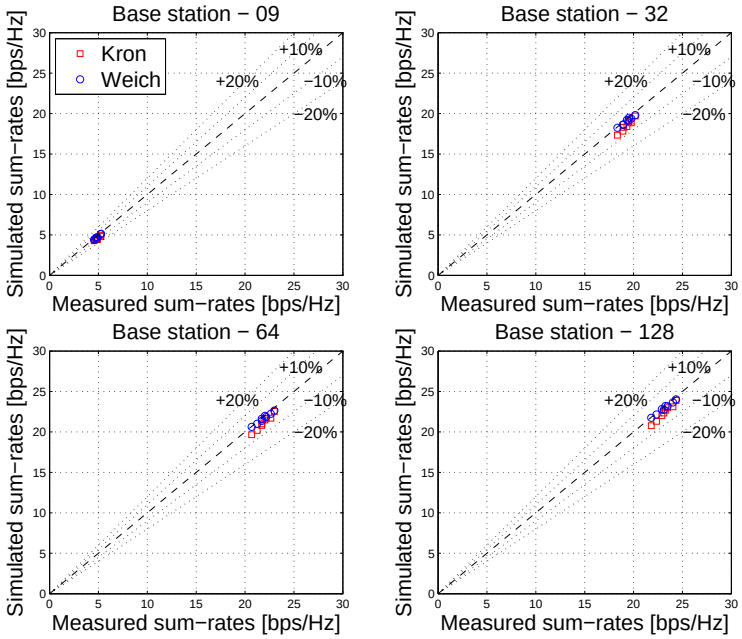

Figure 5.8: The Zero-forcing sum-rates of Measured versus Modeled for the measurement campaign "UCA with 9 synchronized users - indoor" at a E_s/N_0 of 10 dB.

The ZF sum-rates computed from the last measurement campaign for both the Kronecker model and the Weichselberger model are shown in Figure 5.8. It can be observed that the Weichselberger model fits the measurements best with no model error for 9, 32, 64 and 128 antennas, respectively. The Kronecker model underestimates the measured ZF sum-rate, when having more than 9 antennas. When the number of antennas is 9, the Kronecker model performs very well, that reflects it is a good model in this case.

It is also to interesting to study the significant increase of the ZF sum-rate for both models, as the BS antenna is larger than 9. Also, the reason for this is because ZF pre-coder is used to remove ISI and this process needs

to consume power, however, the consumption reduces, as the number of antenna elements at BS increases.

In the end, two comments for this chapter are given by

- Firstly, in the literature [15], it has been shown that the Kronecker model performs poorly, when having larger antennas (>3). However, the Kronercker model shows good match for equipping more antennas at BS, when considering UCA scenarios.
- Second, for massive MIMO channels performed with UCA, both the Kronverker model and the Weichselberger are good model for performance analysis and evaluation.

Chapter 6

Random Cluster Model

To model the massive MIMO channel based on the Random Cluster Model (RCM) [16], we use the measurement data from the measurement campaign "ULA with 5 virtual users" with the linear array. In this chapter, the measurement data processing, the implementation of the RCM as well as the channel behavior and validation will be present.

6.1 Measurement Data Processing

Instead of investigating the measured channel matrix, i.e., the correlative models, the RCM is modeled on a cluster level. The space-alternating generalized expectation maximization(SAGE) algorithm [23] is applied to estimate the MPCs of the raw data obtained from the measurement. With joint clustering and tracking, the MPCs having similar azimuth angles, elevation angles and delays are grouped into one cluster by using KPower-Means clustering algorithm [24]. To extract the clusters better, a sliding window with 10 adjacent antennas over the ULA was implemented.

6.2 Parametric Model

Each of the extracted clusters contains a set of parameters to classify the cluster location, power, spread, number of the MPCs in each cluster and its updating over time. The impulse response of the channel can be written as the sum of the cluster impulse responses:

$$\mathbf{H}(t, f) = \sum_{c=1}^{N_c} \mathbf{H}_c(t, f, \mathbf{\Theta}_c) \tag{6.1}$$

where $\mathbf{H}_c$ expresses the impulse response of the cth cluster, the cluster parameter set $\mathbf{\Theta}_c$ contains the mean azimuth and elevation angles for both

receive and transmit side $\bar{\varphi}_{\mathrm{Rx}}, \bar{\varphi}_{\mathrm{Tx}}, \bar{\theta}_{\mathrm{Rx}}, \bar{\theta}_{\mathrm{Tx}}$, the mean delay $\bar{\tau}_c$, the spread of preceding parameters $\sigma_{\varphi_{\mathrm{Rx}},c}, \sigma_{\varphi_{\mathrm{Tx}},c}, \sigma_{\theta_{\mathrm{Rx}},c}, \sigma_{\theta_{\mathrm{Tx}},c}, \sigma_{\tau,c}$, the cluster power $\sigma^2_{\gamma,c}$, the number of MPCs within cth cluster $N_{c,p}$, the number of coexisting cluster per snapshot N_c, the total snapshot power ρ_c and the cluster lifetime Λ_c. To simulate a smoothly time-variant channel over the large array, the rate of change parameters $\triangle\bar{\varphi}_{\mathrm{Rx},c}, \triangle\bar{\varphi}_{\mathrm{Tx},c}, \triangle\bar{\theta}_{\mathrm{Rx},c}, \triangle\bar{\theta}_{\mathrm{Tx},c}, \triangle\bar{\tau}_c, \triangle\sigma^2_{\gamma,c}$ are included in the clsuter parameter set $\mathbf{\Theta}_c$. The cluster impulse response is given as

$$\mathbf{H}(t, f, \mathbf{\Theta}_c) = \sum_{p=1}^{N_c,p} \mathbf{H}_{cp}(t, f, \mathbf{\Theta}_{cp}) \tag{6.2}$$

where the impulse response of the pth MPC in the cth cluster is denoted by $\mathbf{H}_{cp}$. Each cluster consists of $N_{c,p}$ MPCs, and each MPC parameter set $\mathbf{\Theta}_{cp}$ is composed by the MPC amplitude $\gamma_{c,p}$, delay $\tau_{c,p}$, azimuth and elevation angles $\varphi_{\mathrm{Rx},c,p}, \varphi_{\mathrm{Tx},c,p}, \theta_{\mathrm{Rx},c,p}, \theta_{\mathrm{Tx},c,p}$.

As discussed in 1.2.2, one obvious feature of RCM improved from the COST 273 model is that the environment PDF was employed to describe the channel properties. The environment PDF $\mathbf{\Theta}_{\mathrm{env}}$, which is the joint distribution of entire cluster parameters, is given by

$$\begin{aligned}\mathbf{\Theta}_{\mathrm{env}} =& p(\mathbf{\Theta}_c) \\ =& p(\bar{\varphi}_{\mathrm{Rx}}, \bar{\varphi}_{\mathrm{Tx}}, \bar{\theta}_{\mathrm{Rx}}, \bar{\theta}_{\mathrm{Tx}}, \bar{\tau}_c, \sigma_{\varphi_{\mathrm{Rx}},c}, \sigma_{\varphi_{\mathrm{Tx}},c}, \sigma_{\theta_{\mathrm{Rx}},c}, \sigma_{\theta_{\mathrm{Tx}},c}, \sigma_{\tau,c}, \sigma^2_{\gamma,c}, \\ & \rho_c, N_c, N_{c,p}, \triangle\bar{\varphi}_{\mathrm{Rx},c}, \triangle\bar{\varphi}_{\mathrm{Tx},c}, \triangle\bar{\theta}_{\mathrm{Rx},c}, \triangle\bar{\theta}_{\mathrm{Tx},c}, \triangle\bar{\tau}_c, \triangle\sigma^2_{\gamma,c}, \Lambda_c)\end{aligned} \tag{6.3}$$

In this thesis work, a kernel density estimator toolbox for MATLAB [25] is used to estimate the environment PDF. Since all the cluster parameters are obtained from the raw measurement data, the environment PDF can closely reflects the real environment with its multivariate PDF description.

The primary job of the parametric model is to generate the cluster parameter sets $\mathbf{\Theta}_c$ and MPC parameter sets $\mathbf{\Theta}_{cp}$ from the environment PDF $\mathbf{\Theta}_{\mathrm{env}}$. Once the environment PDF $\mathbf{\Theta}_{\mathrm{env}}$ has been obtained , a set of cluster parameter for one snapshot (refer to a sliding window in our thesis work) will be determined by using the marginal PDF and conditional PDF. The rough procedure is given as

- Number of clusters for the first window N_c is drawn from the marginal PDF $P(N_c)$, which is computing by integrating all cluster parameters except for N_c of the environment PDF.

- With the fixed N_c, the second obtained parameter window power ρ_c is determined with its marginal PDF conditioned on the N_c, $P(\rho_c|N_c)$.

- Based on the environment PDF conditioned on ρ_c and N_c, the cluster parameter set $\mathbf{\Theta}_c$ is generated.

After that, we create the MPC parameter sets $\mathbf{\Theta}_{cp}$ by using the generated $\mathbf{\Theta}_c$. The MPC amplitude is defined as

$$|\gamma_{c,p}| = \sqrt{\frac{\sigma^2_{\gamma,c}}{|\gamma_{att}|^2 N_{c,p}}} \tag{6.4}$$

which is the cluster power divided by the number of the MPCs in the current cluster, the phase of $\gamma_{c,p}$ follows the uniform distribution $\mathbf{U}(-\pi\ \pi)$, and $|\gamma_{\text{att}}|^2$ is the cluster attenuation factor aiming to fading in and out clusters smoothly over the large array. The MPC angle parameters $\varphi_{\text{Rx},c,p}, \varphi_{\text{Tx},c,p}$, $\theta_{\text{Rx},c,p}, \theta_{\text{Tx},c,p}$ are generated by Gaussian distribution, that is

$$\begin{aligned}
\varphi_{\text{Rx},c,p} &\sim \mathcal{N}(\bar{\varphi}_{\text{Rx}}, \sigma^2_{\varphi_{\text{Rx}},c}) \\
\varphi_{\text{Tx},c,p} &\sim \mathcal{N}(\bar{\varphi}_{\text{Tx}}, \sigma^2_{\varphi_{\text{Tx}},c}) \\
\theta_{\text{Rx},c,p} &\sim \mathcal{N}(\bar{\theta}_{\text{Rx}}, \sigma^2_{\theta_{\text{Rx}},c}) \\
\theta_{\text{Tx},c,p} &\sim \mathcal{N}(\bar{\theta}_{\text{Tx}}, \sigma^2_{\theta_{\text{Tx}},c})
\end{aligned} \tag{6.5}$$

The mean and the variance of the Gaussian distribution is the mean angle and angle spread of the current cluster, respectively. The generated parameter set is for the first sliding window, and the next windows repeat the same step. The parameter updating per window as well as the cluster appear and disappear on the antenna array will be realized by a birth-death process, detailed description in next section.

6.3 Birth-Death Process

One significant feature of the cluster models is that a time-variant channel is modeled, here we apply time-variation modeling concept to the spatial domain. The RCM considers a birth-death process to update the parameters every sliding window aiming to generate a smoothly space-variant radio channel along the large array. The cluster parameters updating over the large array are achieved by the rate of change parameters.

For the rate of change cluster parameters, we define them as the slopes of the parameter change along the array. For instance, the cluster power variations for a LOS scenario (MS 3) and a NLOS scenario(MS 5) are shown in Figure 6.1.We fit each of them by a dotted linear line to get the slope, which is considered as the rate of change of cluster power $\triangle\sigma^2_{\gamma,c}$. The other rate of change parameters, i.e., angles and delay, are realized in the same way.

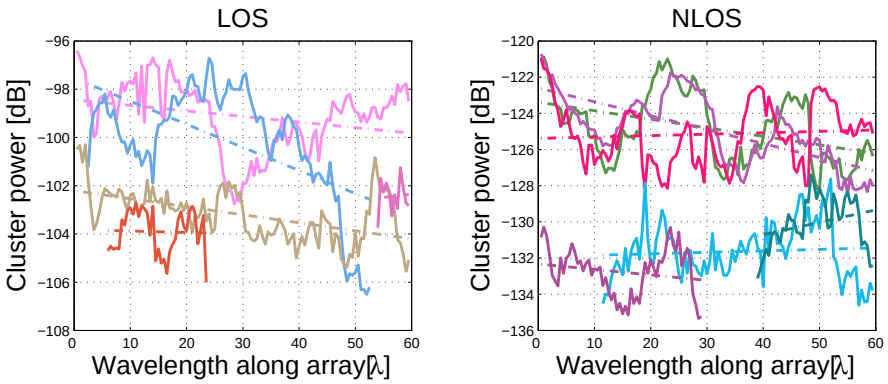

Figure 6.1: The cluster power variations along the array

The power variations for LOS scenario (left side of Figure 6.1) only contains the NLOS clusters. The LOS component are considered separately by using the Ricean k-factor, which is defined as the ratio of power between the LOS component and NLOS clusters.

Since the ULA performed at the BS has a physically large dimension, the massive MIMO channels can have observable variation over the large array. The procedure of clusters accrue and pass away on the large array called birth-death process. We determine the birth and death rate form the measurement data, by counting the number of newly born and died clusters per sliding window, shown in Figure 6.2.

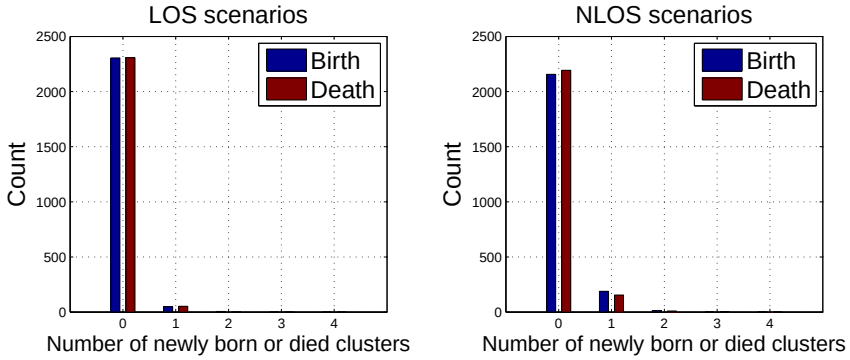

Figure 6.2: Cluster birth and death per sliding window along the large array.

The two histograms give the statistic data of all LOS and NLOS scenarios from the measurement campaign "ULA with 5 virtual users" separately, where the users located in measurement sites MS 1-4 having LOS condition and sites MS 5-8 having NLOS condition (see Figure 2.2). The birth and

death rate are computed from Figure 6.2 shown in Table 6.1. It is noteworthy that the the count for the birth and death is huge when no fresh cluster born or die. Furthermore, the NLOS scenarios present a higher birth rate and death rate due to the rich scattering propagation environment.

	LOS [birth/death]	NLOS [birth/death]
0 cluster	0.9771/0.9975	0.9136/0.9292
1 cluster	0.0203/0.0225	0.0797/0.0657
2 clusters	0.0026/0	0.0059/0.0042
3 clusters	0/0	0.0004/0.0009
4 clusters	0/0	0.0004/0

Table 6.1: Birth-death rate.

In this thesis work, the birth of a new cluster is governed by the cluster birth rate. For a new-born cluster, the cluster parameter set $\mathbf{\Theta}_c$ is gained from the environment pdf $\mathbf{\Theta}_{\text{env}}$ by repeating the procedure in the parametric model. With the obtained cluster lifetime Λ_c, the cluster disappears as its lifetime has terminated.

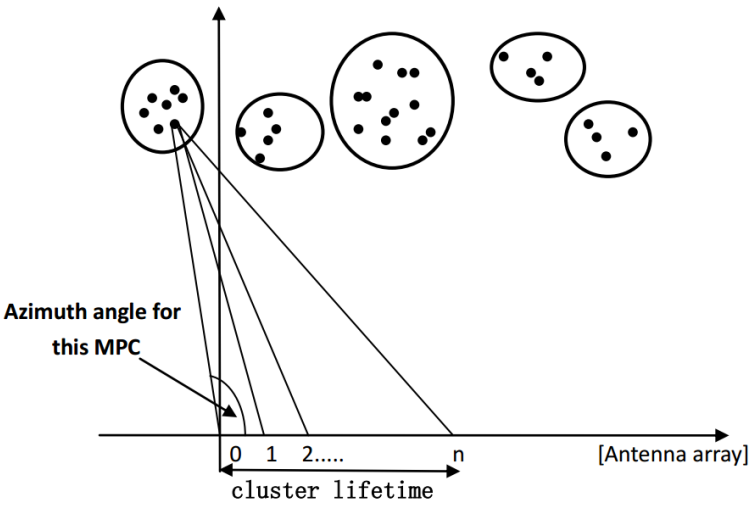

Figure 6.3: MPC parameter updating.

The parameter updating talked previously is on the cluster level along its cluster lifetime Λ_c. For the MPCs parameter change over the antenna array, the updated MPC amplitude $\gamma_{c,p}$ is given as

$$|\gamma_{c,p}^{n+1}|^2 = |\gamma_{c,p}^{n}|^2 + \triangle\sigma_{\gamma,c}^2 \frac{\lambda}{2} \tag{6.6}$$

where $\triangle\sigma_{\gamma,c}^2$ is the rate of change of cluster power, $\frac{\lambda}{2}$ is the distance of two adjacent antenna element. The MPC delay $\tau_{c,p}$ is refreshed by establishing a coordinate system (see Figure 6.3). The MPC position is represented by its coordinate $(\cos\varphi_{\mathrm{Rx},c,p} d_{c,p}, \sin\varphi_{\mathrm{Rx},c,p} d_{c,p})$. And $d_{c,p}$ is the distance between the MPC and the BS array, which is calculated by multiplying the MPC delay $\tau_{c,p}$ by the speed of light. And the $\varphi_{\mathrm{Rx},c,p}$ is the azimuth angle at receiver side obtained in Section 6.2. After given the coordinate of the MPC, the $d_{c,p}$ can be determined for the each antenna consisted in its lifetime.

6.4 System Model

According to the cluster parameters and MPC parameters generated before, the system model can be written as

$$\mathbf{H}(t,f) = \sum_{c=1}^{N_c} \sum_{p=1}^{N_{c,p}} \gamma_{c,p} \mathrm{a}_{\mathrm{Rx}}(\varphi_{\mathrm{Rx}}, \theta_{\mathrm{Rx}}) \mathrm{a}_{\mathrm{Tx}}^{T}(\varphi_{\mathrm{Tx}}, \theta_{\mathrm{Tx}}) e^{-j2\pi f \tau_{c,p}} \tag{6.7}$$

where $\mathrm{a}_{\mathrm{Rx}}(\varphi_{\mathrm{Rx}}, \theta_{\mathrm{Rx}})$ is the receive array steering vector and $\mathrm{a}_{\mathrm{Tx}}(\varphi_{\mathrm{Tx}}, \theta_{\mathrm{Tx}})$ is the transmit array steering vector. And $N_c, N_{c,p}$ are the number of the cluster per snapshot and the number of MPCs in cth cluster, respectively. $\tau_{c,p}$ is the delay for each MPC in cth cluster. Here we have omni-directional antennas at the BS, the array steering vector equals to 1. And the phase different was embodied in the MPCs delay updating. We can rewrite the system model as

$$\mathbf{H}(t,f) = \sum_{c=1}^{N_c} \sum_{p=1}^{N_{c,p}} \gamma_{c,p} e^{-j2\pi f \tau_{c,p}} \tag{6.8}$$

For the LOS scenario simulation, the direct propagation path LOS component achieved by Ricean k-factor is considered as a special cluster consisted of only one MPC, and the lifetime Λ_c of the LOS cluster is assumed as the whole linear array.

6.5 Model Validation

To validate the simulated model, a number of scalar properties showing the channel performance are introduced, i.e., the spatial and statistic auto-

correlation, large scale fading, moreover, the simulation results for the scalar properties will also be shown in this section. The LOS and NLOS scenarios are modeled separately, since the statistic data both from the measurement and simulation show different characteristics for the two propagation conditions.

6.5.1 Spatial Auto-Correlation

The spatial auto-correlation indicates correlation of a variable with itself through space. Furthermore, we here use it to show the correlation between each antenna elements over the antenna array. The correlation coefficient for one realization is defined as

$$r(\triangle j) = \left| \frac{1}{L} \sum_{\ell=1}^{L} \frac{1}{K} \sum_{k=1}^{K} \frac{1}{J} \sum_{j=1}^{J} \frac{h_{k,j,\ell} h^*_{k,j+\triangle j,\ell}}{|h_{k,j,\ell}||h_{k,j+\triangle j,\ell}|} \right| \tag{6.9}$$

where $h_{k,j,\ell}$ is the channel gain at kth user, jth antenna and ℓth subcarrier. $\triangle j$ represents the antenna space along the array.

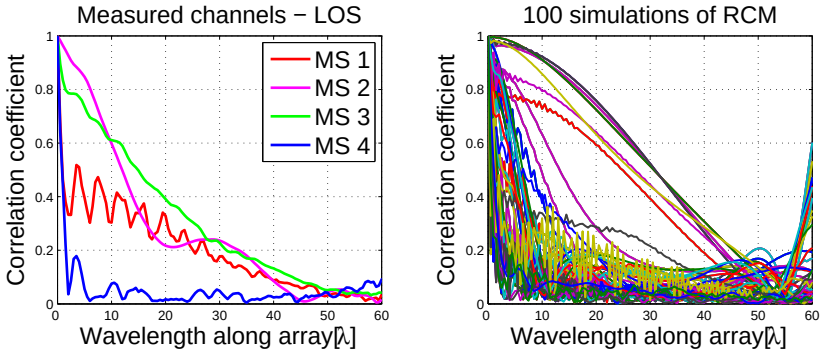

Figure 6.4: The spatial auto-correlation comparision between the measured and simulated channel (LOS scenarios).

Figure 6.4 gives the auto-correlation of measured channel and the simulated channel when we model the LOS conditions. In the left of the figure, it is easy to find the MS 2 and MS 3 are stronger than the MS 1 and MS 4, and the correlation coefficient becomes smaller as the wavelength increases. As can be seen in the right of the figure, the RCM leads to the same performance as the measured channels.

However, we must point out the correlation coefficient goes to higher value at the end of the array, that is because the data volume achieved in the end of the array is more less than that achieved in the previous array.

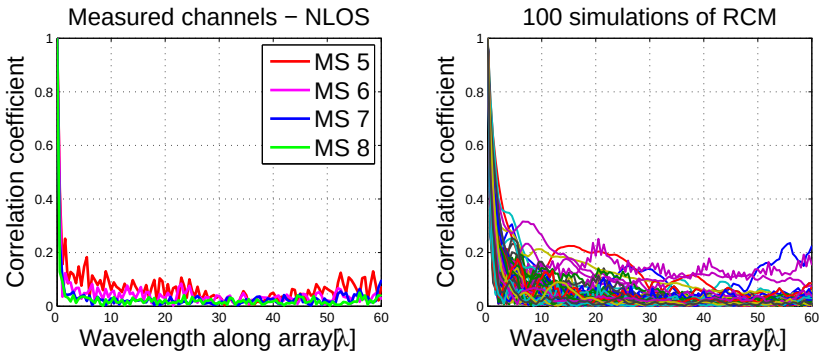

Figure 6.5: The spatial auto-correlation comparision between the measured and simulated channel (NLOS scenarios).

On the other hand, the simulation times is not enough due to the time constraints.

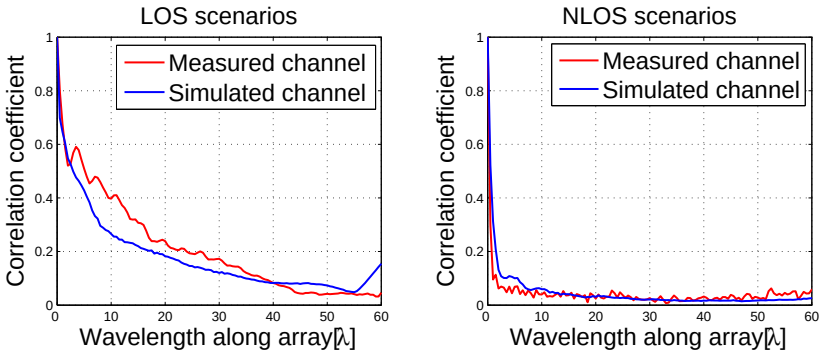

Figure 6.6: The averaged spatial auto-correlation comparision between the measured and simulated channel.

According to the left of Figure 6.5, we can see that the correlation coefficient for the NLOS conditions always goes to smaller after a few wavelength if consider the measured channels, since the scatterers in the environment can support strong decorrelation effect to the channel. The same characteristics is given for the model channel, as illustrated in the right of the figure. As mentioned in the last paragraph, the simulation times for this are also not enough.

In the Figure 6.6 we plot the average spatial auto-correlation of the LOS scenarios and the NLOS scenarios for the measured channel and the simulated channel. Both the LOS scenarios and the NLOS scenarios show a smaller gap between the measured channel and the simulated channel.

Therefore, the RCM can reflect the measured channel if considering the spatial auto-correlation scale.

6.5.2 Statistic Auto-Correlation of Fading Process

Another important property to construct and evaluate a channel model is the statistic auto-correlation between the channel parameters, e.g., channel fading. A wide-sense stationary (WSS) channel is assumed, where μ and σ^2 are the mean and variance of each realization, the correlation coefficient is given as

$$R(\tau) = \frac{E[(x_t - \mu)(x_{t+\tau} - \mu)]}{\sigma^2} \tag{6.10}$$

where E represents the expected value, τ is the antenna space over the ULA performed at BS.

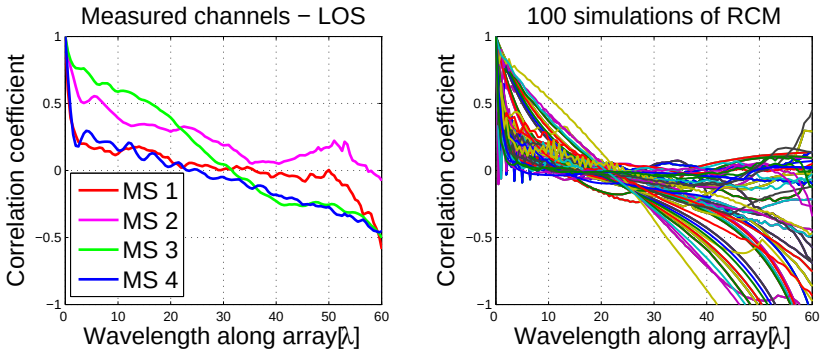

Figure 6.7: The statistic auto-correlation of fading (LOS scenarios).

By using the statistic auto-correlation for the channel power, the correlation coefficient can be obtained, as illustrates in Figure 6.7 and Figure 6.8.

Figure 6.7 shows the statistic auto-correlation of the measured channels and the modeled channels, and according to the left of the figure, it can be observed that the correlation coefficient becomes smaller as the wavelength. From the right of the figure, we can know that the correlation coefficient for all simulated realization of RCM decreases with the increase of the wavelength. However, we must tell the truth that some of the realizations have the lower correlation coefficient, which is smaller than -1. That indicates that we still need do many more simulations.

In the left of Figure 6.8, it is clear that all NLOS scenarios own a constant correlation coefficient after a few wavelength. Because the data volume of the end array is more less than that of the previous array, the correlation coefficient becomes higher at the end of the array. The same

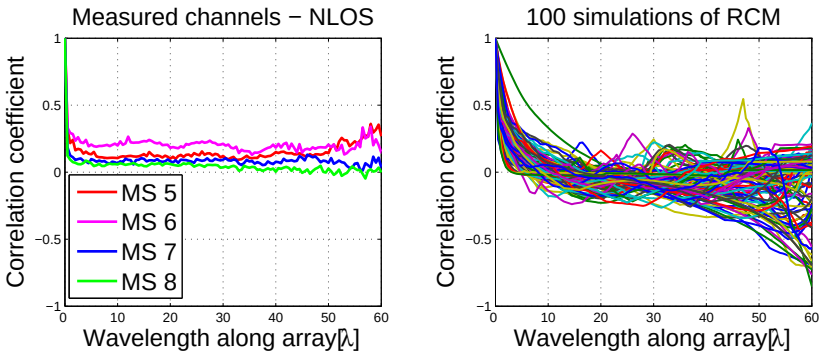

Figure 6.8: The statistic auto-correlation of fading (NLOS scenarios).

trend for the simulated channel is shown in the right of the figure, and then we can state that the RCM closely follows the measured when the statistic auto-correlation is considered.

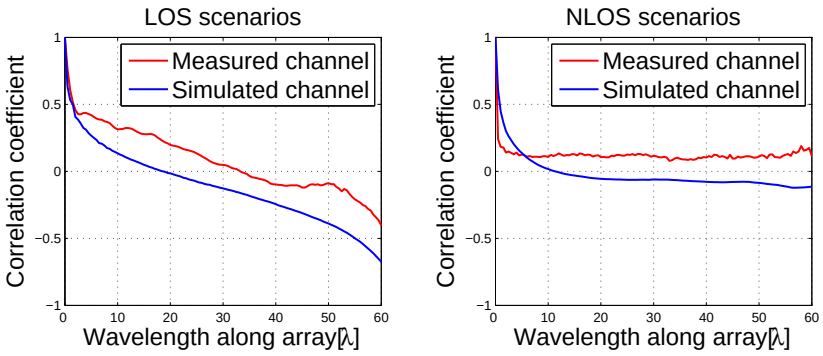

Figure 6.9: The averaged statistic auto-correlation of fading.

Averaging all the realizations for the measured channel and the simulated channel, the Figure 6.9 can be obtained. From the figure,we are motivated to study the gap between the measured channel and the measured channel. Despite the gap is too bigger, it can be accepted due to the limited simulation times.

6.5.3 Large-Scale Fading

The large-scale fading along the measured antennas is evaluated by the following equation:

$$\mathbf{P}_{\mathrm{LSF}} = \max |\mathbf{P}_{\mathrm{ant}} - \mathbf{P}_{\mathrm{Mean}}| \tag{6.11}$$

where $\mathbf{P}_{ant}$ is the power on each antenna and $\mathbf{P}_{Mean}$ is the average power over the large array. In order to check the stationary, we search for the antenna with the higher fluctuation.

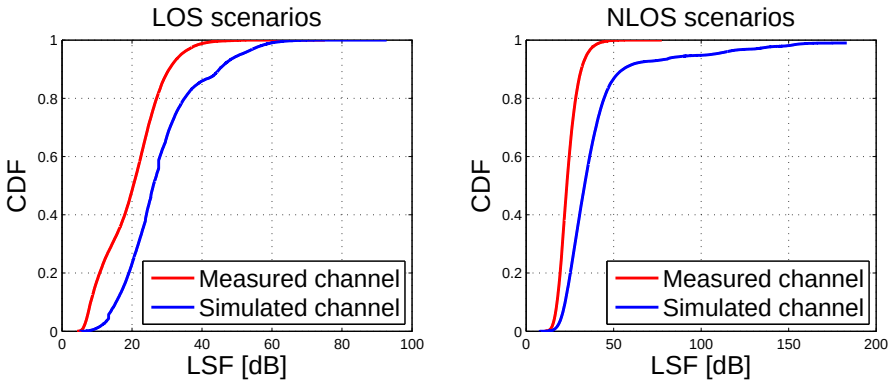

Figure 6.10: Comparison between CDFs of the large scale fading.

As shown in Figure 6.10, on one hand, it is easy to observe that the CDF curve of the simulated channel has a longer upper tail than the measured channel when considering the LOS scenarios and the NLOS scenarios. On the other hand, since the CDF curve of the measured channel is more steeper than the simulated channel for both kinds of scenarios, the measured channel is more stable than RCM. The gap between the measured channel and the simulated channel is bigger, as the simulation times for the simulated channels are not enough because of the time restriction.

Chapter 7

Conclusions and Discussion

This thesis has investigated the correlative models and the cluster model for massive MIMO by using measured channels.

Conclusion and summary for the correlative models are as follows:

- With physically-large array, both the uplink capacity and the ZF sum-rates achieved in the correlative models underestimate those achieved in the real-life channel. Furthermore, the Weichselberger model is more accurate than the Kronecker model. Singular value spreads were gathered for different scenarios, and they indicates that the correlative models cannot do a good job of representing the real-life channel. The worse match is because of the physically large array.

- With compact cylindrical array and closely-spaced users, we deliver several conclusions for the correlative models, that is, (i) the correlative models match well with real-life data. (ii) Both the uplink capacity and the ZF sum-rate not only are influenced by rapidly changing environment (following the second measured campaign), but also give higher values for the LOS scenarios when compared with NLOS scenarios (following the third measurement campaign). (iii) We found that for compact array and closely-spaced users, the correlative models can be used for analytical study and the further problem is that large number of parameters in correlation matrix is a modelling challenge.

To the end, the RCM employed a statistical description (namely environment PDF) of the measured scenarios to generate clusters for the modelled scenario. Expect for that, we used the Birth-death process to model continuously time-varying scenarios and used the K-factor to model the LOS component.

In order to validate the RCM, the spatial auto-correlation, the statistic auto-correlation and the large-scale fading have been examined. Despite

the spatial auto-correlation has shown that the channel correlation give a good match between the RCM and the measured channels, the statistic auto-correlation and the large-scale fading told us that the power match still needs to improve. On the other hand, the simulation times is not enough due to the time constraints.

In future work, it is interesting to consider well-separated users, when investigating the correlative models. And for the RCM, we may do enough simulations so that some better suggestions can be achieved.

References

[1] X. Gao, O. Edfors, F. Rusek, and F. Tufvesson, "Linear pre-coding performance in measured very-large MIMO channels," in *IEEE Vehicular Technology Conference (VTC Fall)*, Sep. 2011.

[2] E. Dahlman, S. Parkvall, J. Skold, and P. Beming, *3G Evolution, Second Edition: HSPA and LTE for Mobile Broadband*, 2nd ed. Academic Press, 2008.

[3] T. Narasimhan, P. Raviteja, and A. Chockalingam, "Large-scale multiuser SM-MIMO versus massive MIMO," in *Information Theory and Applications Workshop(ITA)*, Feb. 2014.

[4] J. Hoydis, S. ten Brink, and M. Debbah, "Massive MIMO in the UL/DL of cellular networks: How many antennas do we need ?" *IEEE Journal on Selected Areas in Communications*, Feb. 2013.

[5] R. Baldemair, E. Dahlman, G. Fodor, G. Mildh, S. Parkvall, Y. Selen, H. Tullberg, and K. Balachandran, "Evolving wireless communications: Addressing the challenges and expectations of the future," *IEEE Vehicular Technology Magazine*, Mar. 2013.

[6] E. Larsson, O. Edfors, F. Tufvesson, and T. Marzetta, "Massive MIMO for next generation wireless systems," *IEEE Communications Magazine*, Feb. 2014.

[7] F. Boccardi, R. Heath, A. Lozano, T. Marzetta, and P. Popovski, "Five disruptive technology directions for 5G," *IEEE Communications Magazine*, Feb. 2014.

[8] H. Q. Ngo, "Massive MIMO: Fundamentals and system designs," Ph.D. dissertation, Linköping University, 2015.

[9] D. Tse and P. Viswanath, *Fundamentals of Wireless Communication*. New York,USA: Cambridge University Press, 2005.

[10] H. Q. Ngo, E. Larsson, and T. Marzetta, "Energy and spectral efficiency of very large multiuser MIMO systems," *IEEE Transactions on Communications*, Apr. 2013.

[11] F. Rusek, D. Persson, B. K. Lau, E. Larsson, T. Marzetta, O. Edfors, and F. Tufvesson, "Scaling up MIMO: Opportunities and challenges with very large arrays," *IEEE Signal Processing Magazine*, Jan. 2013.

[12] S. Wyne, A. Molisch, P. Almers, G. Eriksson, J. Karedal, and F. Tufvesson, "Statistical evaluation of outdoor-to-indoor office MIMO measurements at 5.2 GHz," in *IEEE VTC-Spring*, May 2005.

[13] N. Costa and S. Haykin, *Multiple-input, multiple-output channel models: theory and practice*, ser. Wiley series in adaptive and learning systems for signal processing, communication and control. New York: IEEE, Institute of Electrical and Electronic Engineers Hoboken, N.J. John Wiley, 2010.

[14] W. Weichselberger, M. Herdin, H. Özcelik, and E. Bonek, "A stochastic MIMO channel model with joint correlation of both link ends," *IEEE Transactions on Wireless Communications*, Jan. 2006.

[15] W. Weichselberger, "Spatial structure of multiple antenna radio channels a signal processing viewpoint," Ph.D. dissertation, Technische Universität Wien, Dec. 2003.

[16] N. Czink, "The random-cluster model - a stochastic MIMO channel model for broadband wireless communication systems of the 3rd generation and beyond," Ph.D. dissertation, Technische Universität Wien, 2007.

[17] X. Gao, O. Edfors, F. Rusek, and F. Tufvesson, "Massive MIMO performance evaluation based on measured propagation data," *IEEE Transactions on Wireless Communications*, July 2015.

[18] X. Gao, F. Tufvesson, O. Edfors, and F. Rusek, "Measured propagation characteristics for very-large MIMO at 2.6 GHz," in *Conference Record of the 46th Asilomar Conference on Signals, Systems and Computers (ASILOMAR)*, Nov. 2012.

[19] "D1.2 - MaMi channel characteristics: Measurement results," ULUND, Report, 2015.

[20] J. Flordelis, X. Gao, G. Dahman, F. Rusek, O. Edfors, and F. Tufvesson, "Spatial separation of closely-spaced users in measured massive multi-user MIMO channels," in *IEEE International Conference on Communications*, 2015.

[21] A. Paulraj, R. Nabar, and D. Gore, *Introduction to Space-Time Wireless Communications*, 1st ed. New York,USA: Cambridge University Press, 2003.

[22] X. Gao, M. Zhu, F. Rusek, F. Tufvesson, and O. Edfors, "Large antenna array and propagation environment interaction," in *48th Asilomar Conference on Signals, Systems and Computers*, Nov. 2014.

[23] B. Fleury, M. Tschudin, R. Heddergott, D. Dahlhaus, and K. Ingeman Pedersen, "Channel parameter estimation in mobile radio environments using the SAGE algorithm," *IEEE Journal on Selected Areas in Communications*, Mar. 1999.

[24] N. Czink, P. Cera, J. Salo, E. Bonek, J.-P. Nuutinen, and J. Ylitalo, "A framework for automatic clustering of parametric MIMO channel data including path powers," in *IEEE 64th Vehicular Technology Conference*, Sep. 2006.

[25] A. Ihler, "Kernel density estimation toolbox for MATLAB," http://www.ics.uci.edu/ ihler/code/kde.html, July 2007.

List of Figures

1.1 Transmit correlation only depends on the scattering at the transmit side, and correspondingly, receive correlation only relies on the scattering at the receive side. 4

1.2 The RCM framework 5

2.1 Two large antenna arrays: a) practical uniform cylindrical array (UCA), and b) virtual uniform linear array (ULA). 8

2.2 Overview of the measurement area at the campus of the Faculty of Engineering (LTH), Lund University, Sweden. Two BS large antenna arrays were placed at the same roof of E-building of LTH during the two respective measurement campaigns, 8 MS sites were measured. 9

2.3 UCA with 9 synchronized users - outdoor measurement (a) The measurement area, (b) The users moving randomly in a 5 m diameter circle. 10

2.4 UCA with 9 synchronized users - indoor measurement (a) The measurement area, (b) The users. 11

3.1 The transmit-correlation matrix (left) and the receive-correlation matrix (right). Measurement campaign: ULA with 5 virtual users; User location: MS 2; Propagation condition: LOS. . . . 14

3.2 The transmit-correlation matrix (left) and the receive-correlation matrix (right). Measurement campaign: ULA with 5 virtual users; User location: MS 5; Propagation condition: NLOS. . . 15

4.1 Validation of the Kronecker model. Measurement campaign: ULA with 5 virtual users; User location: MS 2; Propagation condition: LOS. 23

4.2 CDFs of singular values for the 5 users in measured and the Kronecker model channel. Measurement campaign: ULA with 5 virtual users; User location: MS 2; Propagation condition: LOS. 24
4.3 Validation of the Weichselberger model. Measurement campaign: ULA with 5 virtual users; User location: MS 2; Propagation condition: LOS. 24
4.4 CDFs of singular values for the 5 users in measured and the Weichselberger model channel. Measurement campaign: ULA with 5 virtual users; User location: MS 2; Propagation condition: LOS. 25
4.5 Validation of the Kronecker model. Measurement campaign: ULA with 5 virtual users; User location: MS 5; Propagation condition: NLOS. 26
4.6 CDFs of singular values for the 5 users in measured and the Kronecker model channel. Measurement campaign: ULA with 5 virtual users; User location: MS 5; Propagation condition: NLOS. 27
4.7 Validation of the Weichselberger model. Measurement campaign: ULA with 5 virtual users; User location: MS 5; Propagation condition: NLOS. 28
4.8 CDFs of singular values for the 5 users in measured and the Weichselberger model channel. Measurement campaign: ULA with 5 virtual users; User location: MS 5; Propagation condition: NLOS. 28
4.9 Validation of the Kronecker model. Measurement campaign: UCA with 5 virtual users; User location: MS 2; Propagation condition: LOS. 30
4.10 CDFs of singular values for the 5 users in measured and the Kronecker model channel. Measurement campaign: UCA with 5 virtual users; User location: MS 2; Propagation condition: LOS. 31
4.11 Validation of the Weichselberger model. Measurement campaign: UCA with 5 virtual users; User location: MS 2; Propagation condition: LOS. 32
4.12 CDFs of singular values for the 5 users in measured and the Weichselberger model channel. Measurement campaign: UCA with 5 virtual users; User location: MS 2; Propagation condition: LOS. 32

4.13 Validation of the Kronecker model. Measurement campaign: UCA with 5 virtual users; User location: MS 5; Propagation condition: NLOS 33

4.14 CDFs of singular values for the 5 users in measured and the Kronecker model channel. Measurement campaign: UCA with 5 virtual users; User location: MS 5; Propagation condition: NLOS. 34

4.15 Validation of the Weichselberger model. Measurement campaign: UCA with 5 virtual users; User location: MS 5; Propagation condition: NLOS 35

4.16 CDFs of singular values for the 5 users in measured and the Weichselberger model channel. Measurement campaign: UCA with 5 virtual users; User location: MS 5; Propagation condition: NLOS. 35

4.17 Validation of the Kronecker model. Measurement campaign: UCA with 9 synchronized users - outdoor; User location: MS 1; Propagation condition: LOS - Crowd. 37

4.18 CDFs of singular values for the 9 users in measured and the Kronecker model channel. Measurement campaign: UCA with 9 synchronized users - outdoor; User location: MS 1; Propagation condition: LOS - Crowd. 37

4.19 Validation of the Weichselberger model. Measurement campaign: UCA with 9 synchronized users - outdoor; User location: MS 1; Propagation condition: LOS - Crowd. 38

4.20 CDFs of singular values for the 9 users in measured and the Weichselberger model channel. Measurement campaign: UCA with 9 synchronized users - outdoor; User location: MS 1; Propagation condition: LOS - Crowd. 39

4.21 Validation of the Kronecker model. Measurement campaign: UCA with 9 synchronized users - outdoor; User location: MS 1; Propagation condition: LOS - No Crowd. 40

4.22 CDFs of singular values for the 9 users in measured and the Kronecker model channel. Measurement campaign: UCA with 9 synchronized users - outdoor; User location: MS 1; Propagation condition: LOS - No Crowd. 40

4.23 Validation of the Weichselberger model. Measurement campaign: UCA with 9 synchronized users - outdoor; User location: MS 1; Propagation condition: LOS - No Crowd. 41

4.24 CDFs of singular values for the 9 users in measured and the Weichselberger model channel. Measurement campaign: UCA with 9 synchronized users - outdoor; User location: MS 1; Propagation condition: LOS - No Crowd. 42
4.25 Validation of the Kronecker model. Measurement campaign: UCA with 9 synchronized users - outdoor; User location: MS 3; Propagation condition: NLOS - Crowd. 43
4.26 CDFs of singular values for the 9 users in measured and the Kronecker model channel. Measurement campaign: UCA with 9 synchronized users - outdoor; User location: MS 3; Propagation condition: NLOS - Crowd. 43
4.27 Validation of the Weichselberger model. Measurement campaign: UCA with 9 synchronized users - outdoor; User location: MS 3; Propagation condition: NLOS - Crowd. 44
4.28 CDFs of singular values for the 9 users in measured and the Weichselberger model channel. Measurement campaign: UCA with 9 synchronized users - outdoor; User location: MS 3; Propagation condition: NLOS - Crowd. 45
4.29 Validation of the Kronecker model. Measurement campaign: UCA with 9 synchronized users - outdoor; User location: MS 3; Propagation condition: NLOS - No Crowd. 45
4.30 CDFs of singular values for the 9 users in measured and the Kronecker model channel. Measurement campaign: UCA with 9 synchronized users - outdoor; User location: MS 3; Propagation condition: NLOS - No Crowd. 46
4.31 Validation of the Weichselberger model. Measurement campaign: UCA with 9 synchronized users - outdoor; User location: MS 3; Propagation condition: NLOS - No Crowd. 47
4.32 CDFs of singular values for the 9 users in measured and the Weichselberger model channel. Measurement campaign: UCA with 9 synchronized users - outdoor; User location: MS 3; Propagation condition: NLOS - No Crowd. 47
4.33 Validation of the Kronecker model. Measurement campaign: UCA with 9 synchronized users - indoor; BS location: BS 1; Crowd: Yes. 48
4.34 CDFs of singular values for the 9 users in measured and the Kronecker model channel. Measurement campaign: UCA with 9 synchronized users - indoor; BS location: BS 1; Crowd: Yes 49
4.35 Validation of the Weichselberger model. Measurement campaign: UCA with 9 synchronized users - indoor; BS location: BS 1; Crowd: Yes. 50

4.36 CDFs of singular values for the 9 users in measured and the Weichselberger model channel. Measurement campaign: UCA with 9 synchronized users - indoor; BS location: BS 1; Crowd: Yes 50
4.37 Validation of the Kronecker model. Measurement campaign: UCA with 9 synchronized users - indoor; BS location: BS 1; Crowd: No. 51
4.38 CDFs of singular values for the 9 users in measured and the Kronecker model channel. Measurement campaign: UCA with 9 synchronized users - indoor; BS location: BS 1; Crowd: No. 51
4.39 Validation of the Weichselberger model. Measurement campaign: UCA with 9 synchronized users - indoor; BS location: BS 1; Crowd: No. 52
4.40 CDFs of singular values for the 9 users in measured and the Weichselberger model channel. Measurement campaign: UCA with 9 synchronized users - indoor; BS location: BS 1; Crowd: No. 52
4.41 Validation of the Kronecker model. Measurement campaign: UCA with 9 synchronized users - indoor; BS location: BS 3; Crowd: Yes. 53
4.42 CDFs of singular values for the 9 users in measured and the Kronecker model channel. Measurement campaign: UCA with 9 synchronized users - indoor; BS location: BS 3; Crowd: Yes. 54
4.43 Validation of the Weichselberger model. Measurement campaign: UCA with 9 synchronized users - indoor; BS location: BS 3; Crowd: Yes. 55
4.44 CDFs of singular values for the 9 users in measured and the Weichselberger model channel. Measurement campaign: UCA with 9 synchronized users - indoor; BS location: BS 3; Crowd: Yes. 55
4.45 Validation of the Kronecker model. Measurement campaign: UCA with 9 synchronized users - indoor; BS location: BS 3; Crowd: No. 56
4.46 CDFs of singular values for the 9 users in measured and the Kronecker model channel. Measurement campaign: UCA with 9 synchronized users - indoor; BS location: BS 3; Crowd: No. 56
4.47 Validation of the Weichselberger model. Measurement campaign: UCA with 9 synchronized users - indoor; BS location: BS 3; Crowd: No. 57

4.48 CDFs of singular values for the 9 users in measured and the Weichselberger model channel. Measurement campaign: UCA with 9 synchronized users - indoor; BS location: BS 3; Crowd: No. 58

5.1 The uplink capacity of Measured versus Modeled for the measurement campaign "ULA with 5 virtual users" at a E_s/N_0 of 10 dB. 60
5.2 The Zero-forcing sum-rates of Measured versus Modeled for the measurement campaign "ULA with 5 virtual users" at a E_s/N_0 of 10 dB. 60
5.3 The uplink capacity of Measured versus Modeled for the measurement campaign "UCA with 5 virtual users" at a E_s/N_0 of 10 dB. 61
5.4 The Zero-forcing sum-rates of Measured versus Modeled for the measurement campaign "UCA with 5 virtual users" at a E_s/N_0 of 10 dB. 62
5.5 The uplink capacity of Measured versus Modeled for the measurement campaign "UCA with 9 synchronized users - outdoor" at a E_s/N_0 of 10 dB. 63
5.6 The Zero-forcing sum-rates of Measured versus Modeled for the measurement campaign "UCA with 9 synchronized users - outdoor" at a E_s/N_0 of 10 dB. 63
5.7 The uplink capacity of Measured versus Modeled for the measurement campaign "UCA with 9 synchronized users - indoor" at a E_s/N_0 of 10 dB. 64
5.8 The Zero-forcing sum-rates of Measured versus Modeled for the measurement campaign "UCA with 9 synchronized users - indoor" at a E_s/N_0 of 10 dB. 65

6.1 The cluster power variations along the array 70
6.2 Cluster birth and death per sliding window along the large array. 70
6.3 MPC parameter updating. 71
6.4 The spatial auto-correlation comparision between the measured and simulated channel (LOS scenarios). 73
6.5 The spatial auto-correlation comparision between the measured and simulated channel (NLOS scenarios). 74
6.6 The averaged spatial auto-correlation comparision between the measured and simulated channel. 74
6.7 The statistic auto-correlation of fading (LOS scenarios). . . . 75
6.8 The statistic auto-correlation of fading (NLOS scenarios). . . 76
6.9 The averaged statistic auto-correlation of fading. 76

6.10 Comparison between CDFs of the large scale fading. 77

List of Tables

6.1 Birth-death rate. 71

List of Abbreviations

BS	Base Station
CSI	Channel State Information
CDF	Cumulative Distribution Function
DPC	Dirty Paper Coding
EVD	Eigenvalue Decomposition
GSCM	Geometry-based Stochastic Channel Model
LTE	Long Term Evolution
LOS	Line-of-sight
ML	Maximum Likelihood
MIMO	Multiple-input Multiple-output
MPC	Multipath component
MS	Measurement Site
MU-MIMO	Multi-user MIMO
NLOS	Non-line-of sight
OFDM	Orthogonal Frequency Division Multiplexing
PDF	probability density function
PSD	Positive Semi-definite
RCM	Random Cluster Model
SAGE	Space-Alternating Generalized Expectation Maximization
SISO	Single Input Single Output
SNR	Signal to Noise Ratio
UCA	Uniform Cylindrical Array
ULA	Uniform Linear Array
UMTS	Universal Mobile Telecommunication System
VNA	Vector Network Analyzer
WSS	Wide Sense Stationary
ZF	Zero-forcing